DYNAMIC RESPONSE OF VISCOELASTIC SOLIDS DESCRIBED BY IMPLICIT CONSTITUTIVE THEORIES

A Dissertation

by

ALAGAPPAN PONNALAGU

Submitted to the Office of Graduate and Professional Studies of
Texas A&M University
in partial fulfillment of the requirements for the degree of

DOCTOR OF PHILOSOPHY

Chair of Committee,	Kumbakonam R. Rajagopal
Co-Chair of Committee,	Arun R. Srinivasa
Committee Members,	Jay R. Walton
	Anastasia Muliana
Head of Department,	Andreas Polycarpou

May 2015

Major Subject: Mechanical Engineering

ABSTRACT

The aim of this work is to study the impact response of multilayered polymers using a thermodynamically consistent framework. Rather than integral type viscoelastic model, the approach here is based on the idea of two inter penetrating networks, one is permanent and other is transient together with the rate equations for the time evolution of the transient network. The primary hypothesis is that, it is possible to use a two network theory to capture the essential features of a impact response of multilayered polymers and solve the resulting boundary value problem using finite volume scheme.

We first study the impact of layered polymer plate involving small deformation using a thermodynamic framework. The constitutive equations are nonlinear even though the strains are small. Six different protocols involving PU and PC, namely pure PC, pure PU, bilayer(PU/PC and PC/PU) and trilayer(PU/PC/PU and PC/PU/PC) were considered to evaluate the performance of the layering sequence based on the kinetic energy transferred on the wall. The interfaces are assumed to be fully bonded. The material parameters for the model was obtained from the experimental creep data from the literature. The layering of polymers improved the performance of plate depending upon the type of layering sequence. In the one and two dimensional study carried out, the performance was best when a compliant layer is placed between two stiff layers. Whereas, when a stiff layer was placed between two less compliant layer, the performance was worse than bilayer. Finally, a thermodynamically consistent finite deformation model was used to evaluate the impact performance of layered plate involving large deformation. A full scale three dimensional impact analysis was carried out with the thermal phenomena suppressed.

Similar to the small deformation study, six different protocols were considered. The material parameters were obtained from the experimental data from the literature involving strain values above 50%. The overall performance was similar to what has been observed in the small strain model.

DEDICATION

I dedicate this dissertation to my parents, Ponnalagu and Meenal.

ACKNOWLEDGEMENTS

I wish to express the deepest gratitude to my Chair, Prof. K. R. Rajagopal for his belief in me and for the opportunity to pursue this research work. I thank him for all the motivation, support and guidance and his mentorship was extremely helpful in providing a well rounded experience consistent to my teaching career. I am really thankful that he was available with thoughtful and kind advices whenever I needed them the most.

I wish to convey sincere thanks to my Co-Chair, Prof. A. R. Srinivasa for constantly conveying the spirit of excitement and enthusiasm in regard to research. I am deeply thankful for the amount of time spent by him for those thought provoking discussions. His guidance was highly rewarding in enhancing my knowledge in the subject and in providing a proper shape and direction to this research.

I was most fortunate to work along with these two mentors and I hope I can continue my academic life with the research values that they have given to me.

My sincere thanks to the Doctoral Committee members, Dr. J. R. Walton, Dr. A. H. Muliana for the insightful comments and support for the successful completion of this work.

Heartfelt thanks to my friends Sudharsan Parthasarathy, Kaarthik Sundar, Jayavel Arumugam for a wonderful time along the way and for being there whenever I needed help in the research work. My stay at College Station was made memorable by many friends and roommates over the last couple of years. Thanks to all of them for the good support, whether near or far away: Mukilan Loganathan, Manojkumar Rangasamy, Jayanth Jayaraman, Manoj Prasad, Rajesh Kumar Boovaragamoorthy, Aravinda Bharathi, Dr. Shreyas Balachandran, Dr. Siva Sankar and so many more.

I am grateful to my family for their support in the last few years, for taking care of many issues so I could continue this pursuit without major difficulties.

TABLE OF CONTENTS

Page

LIST OF FIGURES

FIGURE Page

LIST OF TABLES

TABLE Page

1. INTRODUCTION

Polymers are now-a-days widely used in various engineering fields due to its characteristics such as light weight, transparency and impact resistance. For example, in automobile industry it is used in the manufacture of bumper since it can dissipate large amount of energy when subjected to impact. In addition, providing a coating of polymer throughout the structure serves as effective method for the seismic protection in buildings. It is extensively used in military applications where it is used to increase the blast and ballistic resistance. When it comes to military applications one of the main objective is to protect the individuals, vehicles and structures by reducing the kinetic energy which is transferred to the body. The impact resistant materials are evolving with time, based on the studies conducted in improving their performance. It is necessary to understand the evolution of these materials over the past century to understand the reason for change in type of material used for protection. During the first and the second world wars tanks used were designed, such that it is maneuverable and well protected from the firing. The armors used by soldiers was Rolled Homogeneous Armor(RHA) which is rolled steel plate and structures were protected by using sand bags. The efficiency of the material was evaluated based on the hardness value. In order to increase the protection with the intensity of firing, these materials were made thicker which increased the weight of the tanks and the use of heavy metal in military ground vehicles resulted in reduction in the maximum speed and maneuverability. Meanwhile, RHA's were improved further by using hardened steel, but because of the brittle nature of hardened steel, the plates broke often. Later the soldiers were given manganese-steel body armor but it was also heavy and restricted mobility and in addition it had overheating problem. Next

these manganese were sewn into nylon which protected soldiers from the fragments arising due to the impact. Meanwhile, studies were carried to find armor materials which are non metallic, which resulted in the use of nylon cloth and glass fiber reinforced plastic to provide better ballistic performance which was useful in making plates of different shapes. Of late Kevlar^{TM}is being used commonly in all military departments since it provides protection against fragments and bullets. From the history of these materials it is obvious that, one of the main characteristics which affects the design of armor is the weight. But with the advent of polymers such as PMMA, PC, PU, EVE, etc. for ballistic protection, there has been a huge increase in the use of polymers in armor because of its characteristics such as light weight, impact resistance and transparency. There are also commercial polymers such as PAXCON^{TM}, Dragonshield-HT^{TM}, RhinoArmor^{TM}based on PU, PC, PMMA etc. which are used for the ballistic protection. For example, it can be seen from figures 1.1(a) through 1.1(c) that spraying a coating of RhinoArmor can be used to protect the wall from the impact of a blast. From figure 1.1(d) it can be seen that Dragonshield-HT has been used as protective coating for military vehicles. These can also be used in buildings where conventionally thick layer of cheaper materials are used for protection. Now given the availability of these light weight materials, it is necessary to find efficient ways to further improve the impact performance of these materials.

(a) Wall on the left is coated (RhinoArmor) and wall on right not coated

(b) Blast made in front of the wall

(c) The coated wall does not suffer any serious damage while the uncoated wall is broken completely exposing the interior.

(d) Polyurea coating to protect military vehicle

Figure 1.1: Examples of use of commercial polymers

2. LITERATURE REVIEW AND MOTIVATION

Polymers such as PU, PC, PMMA, EVE have emerged as key materials for armor. The performance of these polymers can be improved further by adopting a appropriate layering sequence and several studies have shown their promise in withstanding both blast and ballistic impacts. For example, Tekalur et al. [35] carried out experiments on a rectangular polymer composite plate made of EVE and PU by impacting it with a projectile using a shock tube. The center of the rectangular plate was subjected to impact and the deflection was measured at the center of the plate for different layering sequence such as trilayer(EVE/PU/EVE), bilayer(EVE/PU) and a individual layer of EVE. The figure 2.1 shows the specimen which is simply supported with one face at the end of shock tube. The results showed that trilayer and bilayer was 100% and 25% better than the individual layer of EVE respectively. In addition, experimental studies by Porter et al. [25] showed the influence of polymer coating on a concrete masonry unit(CMU) subjected to air-blast . When no coating was provided, the CMU shattered into pieces upon impact. However, when one face was coated, it shattered halfway through the thickness, while when it was coated on both the faces it remained intact. Similar studies were carried out by Amini et al. [3] using a gas gun to subject a plate coated with PU to projectile impact. There were no signs of visible failure when the coating was provided whereas when no coating was provided it failed completely. The above experimental studies confirm that the presence of the polymeric material and layering improves the impact performance of structures. With the availability of different types of polymer it is not feasible to conduct experiments for each and every combination of layering sequence and select a optimal sequence. In addition, cost of these experiments are high since it

involves the use of shock tube(see figure 2.2(a)) or gas gun to generate the projectile motion and high speed cameras(see figure 2.2(b)) are needed to record the images to measure the displacement due to impact. Therefore techniques need to be developed to reduce the number of experiments done to study the behavior of these materials when subjected to impact. Hence it is necessary to develop models to study the response of these layered polymers.

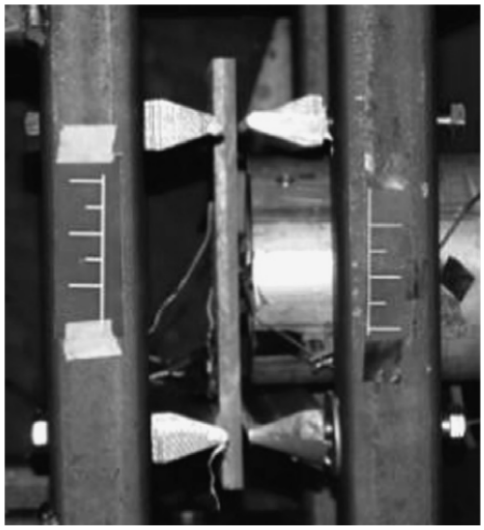

Figure 2.1: Composite plate specimen used by [35]

The key to the performance of polymers is viscoelasticity, which is capable of dissipating large energy with minimal damage. The viscoelastic response of polymers are typically modeled using an integral or differential/rate type approach. In the integral model, the current value of stress is given in terms of an integral of a weighted strain rate history(see Wineman and Rajagopal [38] for example). These weighting kernels are usually expressed as sum of series of exponentials. For example, in a one dimensional response, the typical relaxation kernel is given in terms of a Prony series

Fig. 5. The shock tube facility to produce controlled blast loading.

(a) Shock Tube used for generating projectile motion

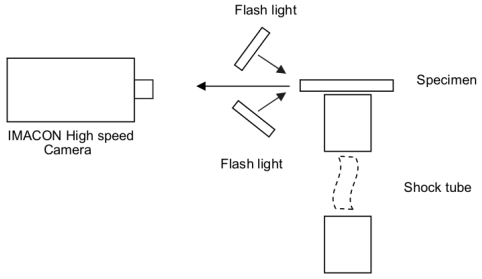

Fig. 8. Schematic of the setup to measure real time deformations in composite plates under blast loadings.

(b) Camera setup for measuring displacement

Figure 2.2: Equipment used in impact experiments

of the form

$$G(t) = 1 + \sum_{i=1}^{N} g_i \exp\left(\frac{-t}{\tau_i}\right) \tag{2.1}$$

where τ_i is the characteristic time, g_i is the normalized amplitude and N represents the number of exponential terms. The number of terms depend upon the nature of the long term relaxation behavior. In a numerical study carried out by Antonakakis et al. [5], 20 terms were required to capture the relaxation response of a polyamide. Even though they were able to capture the relaxation response accurately, the solution was not unique. Knauss and Zhao [22] showed that depending upon the choice of algorithm such as simplified trust region method and trust region method (see MATLAB®), the value of the 20 parameters varied(see the figure 2.3). Furthermore, numerically solving the integral involving the above exponentials is tedious [17]. Nevertheless, experimental and numerical study of impact from a gas gun on a polymer matrix composite was studied using an integral model involving small deformation [8]. The impact response of PU was studied using LS-DYNA [18] by Grujicic et al.; Amini et al.; Amirkhizi et al. [16, 2, 4]. The models discussed above for studying impact use kernels which are known to be highly sensitive or computationally tedious

or both.

Table 1 Coefficients determined by the full trust region method (Matlab) and by the simplified trust region method

i	Simplified trust region method		Trust region method	
	ζ_i seconds	E_∞ MPa	ζ_i seconds	E_∞ MPa
1	10^{-13}	40	4.481×10^{-12}	90
2	5×10^{-13}	40	9.725×10^{-12}	651.8
3	10^{-12}	40	4.581×10^{-11}	19.81
4	10^{-11}	4.438×10^{-14}	9.415×10^{-11}	207
5	10^{-10}	241.5	4.479×10^{-10}	43.83
6	10^{-9}	191	8.558×10^{-10}	143
7	10^{-8}	126.5	6.978×10^{-9}	136.4
8	10^{-7}	100.4	2.912×10^{-8}	22.45
9	10^{-6}	68.39	1.18×10^{-7}	103.4
10	10^{-5}	46.48	1.44×10^{-6}	66.25
11	10^{-4}	40.5	1.184×10^{-5}	38.46
12	10^{-3}	20.69	10^{-4}	42.14
13	10^{-2}	17.48	1.266×10^{-3}	20.77
14	10^{-1}	10.88	0.01071	16.95
15	1	9.009	0.1657	13.45
16	10	5.388	3.278	10.01
17	10^2	5.975	91.77	6.876
18	10^3	10.4	929.3	10.26
		$E_\infty = 69$		$E_\infty = 69.13$

Figure 2.3: Coefficients determined by simplified trust region and trust region method [22]

In contrast to the integral models discussed above, the rate type approach is based on writing a relationship between the stress and its time derivatives and the strain and its time derivatives. This approach involves energy storage and dissipation mechanisms. The models are built based on analogy with one dimensional linear spring and linear dashpots arranged in some combination. In order to accurately capture the long term relaxation behavior, the number of springs and dashpots are increased [19]. The viscoelastic behavior of the polymer subjected to impact was modeled using a three parameter rate type model in LS-DYNA by Shim et al.; Lim

et al.; Ching and Tan [33, 23, 9] and in ABAQUS by Gogineni et al. [15]. The above models are purely mechanistic in nature and are unable to account for the localized heating and other thermal phenomena. It is thus necessary to recast them in a proper thermodynamic framework in order to take into account the coupling between the thermal and mechanical behaviors.

One of the other challenges involved in using these integral/rate type models is the determination of the material parameters. This could be easily understood by considering one dimensional integral and rate type models. The experimental PC creep data [21] obtained from literature was used to determine the parameters for these models. These parameters are obtained by minimizing the error in strain between the experiment and the model using the least square method enforcing that the instantaneous elasticity and the long term creep response match exactly[38] (it is assumed that the experimental creep data obtained from literature has reached the steady state response). The integral model in one dimension is given by

$$\epsilon(x,t) = \int_{-\infty}^{t} J(t-\tau)\frac{\partial \sigma(x,\tau)}{\partial \tau}\, d\tau \tag{2.2}$$

For a instantaneously applied dead load of $P_0 H(t)$ the creep response is given by

$$\epsilon(t) = \epsilon_0 J(t) \tag{2.3}$$

where the typical creep compliance($J(t)$) is given in terms of Prony series of the form

$$J(t) = J_0 + \sum_{i=1}^{N} J_i(1 - \exp(-t/\lambda_i))$$

where 'N' represents the number of terms. It can be observed from figure 2.6 that the fitting of creep data obtained from the literature was possible using a 5 series Prony

which consists of 11 parameters. The response of the rate models can be observed by considering a standard linear solid model (3 parameter) shown in figure 2.4 and a Kelvin-Voigt model in series with a Maxwell model (4 parameter) as shown in figure 2.5. The constitutive equation of the three parameter model is given by

$$\eta_1 \epsilon + \left(\frac{\eta E_2}{E_1 + E_2} \right) \dot{\epsilon} = \ddot{\sigma} + \left(\frac{\eta}{E_1 + E_2} \right) \dot{\sigma} \tag{2.4}$$

where E_1,E_2 and η are material parameters. At constant stress σ_0

$$\epsilon(t) = \frac{\sigma_0}{E_1} + \frac{\sigma_0}{E_2} \left(1 - \exp \left[-\frac{E_2 t}{\eta} \right] \right) \tag{2.5}$$

In the case of the four parameter model the constitutive equation is given by

$$\eta_1 \dot{\epsilon} + \frac{\eta_1 \eta_2}{E_2} \ddot{\epsilon} = \ddot{\sigma} + \left(\frac{\eta_1}{E_2} + \frac{\eta_1}{E_1} + \frac{\eta_2}{E_2} \right) \dot{\sigma} + \frac{\eta_1 \eta_2}{E_1 E_2} \tag{2.6}$$

where E_1,E_2,η_1 and η_2 are material parameters. At constant stress σ_0

$$\epsilon(t) = \frac{\sigma_0}{E_1} + \frac{\sigma_0}{\eta_1} t + \frac{\sigma_0}{E_2} \left(1 - \exp \left[-\frac{E_2 t}{\eta_2} \right] \right) \tag{2.7}$$

The creep response of the three and four parameter models subjected to a constant stress is shown in figure 2.7 and 2.8 respectively. These models do not take into account the thermomechanical phenomena and also the number of parameters required to describe the creep response is higher(11 parameters) and the prediction of the response is not better(see figure 2.7 and 2.8) compared to creep response of the implicit model(see figure 2.9) used in this study (the constitutive equation used in this model will be discussed later). Recently rate type models have been developed by Rajagopal and Srinivasa [29, 30] to describe the viscoelastic response of materials

within a three dimensional thermodynamic framework on the maximization of the rate of entropy production. We however do not consider the thermal aspects of the response and restrict ourselves in this study to purely mechanical response. The framework has two major advantages:

1. The response functions of the model can be easily compared to experimental data and model parameters obtained [30]. We have carried this out for the reported data concerning PU and PC.

2. The resulting set of differential equation is easily amenable to numerical scheme.

The resulting combinations of balance laws and constitutive equations cannot be written in terms of kinematical variables alone and are not amenable to analytical solutions. Moreover, numerical solutions need to interpolate both stresses and displacement independently. As we discuss below finite volume methods offer an attractive approach for solving these equations while maintaining fidelity to the underlying physics.

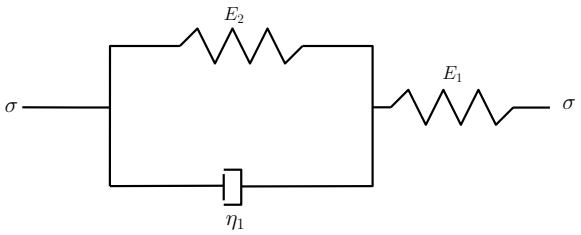

Figure 2.4: Standard linear solid model (three parameter)

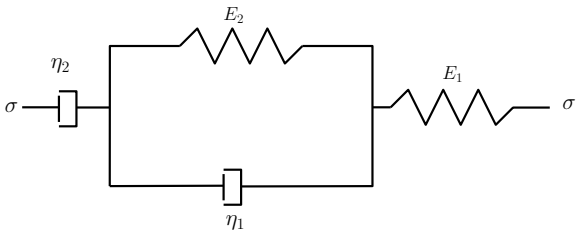

Figure 2.5: Burgers' Model (four parameter)

Finite element method(FEM) is widely used in solid mechanics, whereas finite volume method(FVM) is widely used in fluid mechanics. Unlike FEM, the FVM

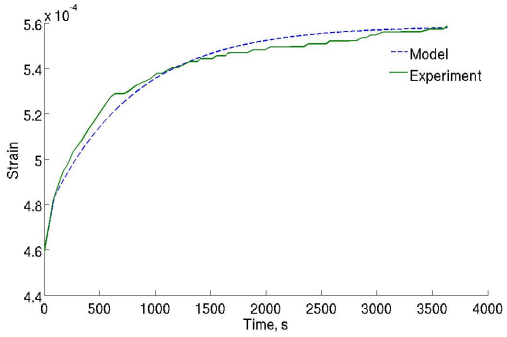

Figure 2.6: Experiments on PC[21] compared with the prony series(11 parameters) is presented here

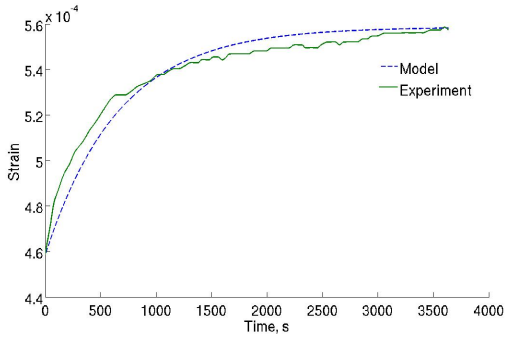

Figure 2.7: Experiments on PC[21] compared with the three parameter model is presented here

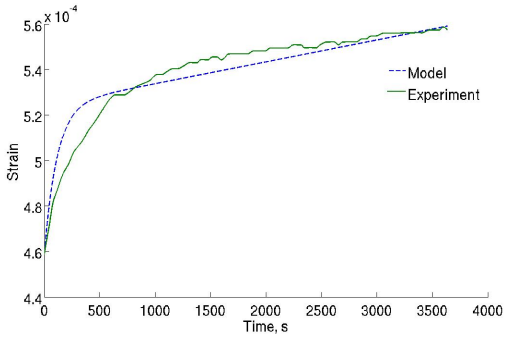

Figure 2.8: Experiments on PC[21] compared with the four parameter model is presented here

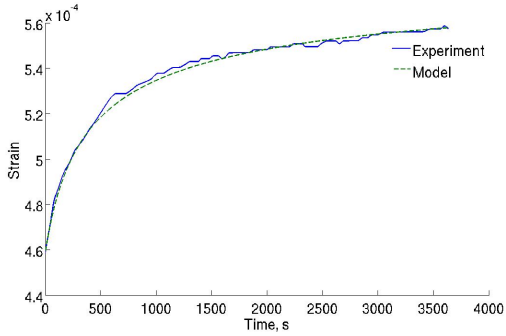

Figure 2.9: Experiments on PC[21] compared with the implicit model (four parameter) is presented here

offers a convenient way to separate the satisfaction of the balance laws and the treatment of constitutive relations. This is especially useful for the implicit models that we consider here since there is no explicit representation for the stress in terms of the kinematical variables and so it is not possible to utilize only kinematical variables as unknowns as routinely done in FEM implementation of the response of solids. The additional characteristics of FVM are [10, 7, 37, 12]

1. It is simple and efficient

2. The method is conservative on local and global scale

3. It is simple to prescribe the boundary conditions

Furthermore, discussion below shows that FVM has also been used to study problems in solid mechanics. Fryer et al. [14] used the control volume(CV) approach to solve two dimensional elastic stress-strain equations. By using the CV approach he was able to solve for displacements directly and also used this approach to solve the axisymmetric problems. Later Bailey and Cross [6] extended the work of Fryer for three dimensional domain involving unstructured meshes. Wheel [37] carried out studies on use of FVM to solve axisymmetric problems. The stress equilibrium equations in terms of the displacement gradient was obtained by using the linear elastic constitutive equations and linear interpolations was used for the gradients. This procedure was also extended to solve small strain problems in linear viscoelastic solids to be used in applications involving heating or cooling of viscoelastic materials. Fainberg and Leister [13] used two dimensional FVM to solve thermal stress problems in anisotropic materials such as semiconductors. Demirdžić et al. [11] used FVM for the stress analysis of the orthotropic bodies. This method was also used to study the small strain response of viscoelastic materials including the thermal effects. The constitutive relation involves the stress which is expressed as integral of the strain history and a relaxation kernel and FVM was used to solve the momentum and energy balance equations [10]. Slone et al. [34] studied the dynamical structural response of linear elastic solids using three dimensional FVM and an implicit scheme for the time step. The discretization method was similar to the previous studies. Studies have been carried out to predict the linear elastic behavior of a incompressible elastic solid by using the finite volume method [7, 36]. This method was used to discretize the momentum balance and kinematic condition of incompressibility and hence the

three dimensional small strain problem was solved using an algorithm similar to SIMPLE^{TM}[24]. Studies discussed above used FVM to solve either linear elastic or linear viscoelastic solid problem.

The Finite volume method(FVM) will be used in this study to numerically solve the governing equations. In this procedure, the whole domain is divided into a finite number of non-overlapping control volumes. For each control volume, the mass, momentum and energy balance equations are exactly met. The constitutive equations are approximated by suitable interpolation schemes across neighbors. With this approach, it is possible to meet local conservation of mass, energy and momentum and only the response functions are approximated.

The hypothesis in this study is that, it is possible to use a two network theory to capture the essential features of a impact response of multilayered polymers and solve the resulting boundary value problem using finite volume scheme.

3. OBJECTIVE AND SCOPE

The primary objective of this dissertation is to study the response of multilayered polymers subjected to impact. A newly developed implicit constitutive framework developed by Rajagopal and Srinivasa [26, 27, 30] has been used to model the response of the layered polymers. Six different protocols namely pure PC, pure PU, bilayer(PU/PC and PC/PU), trilayer (PU/PC/PU and PC/PU/PC) are considered and the performance is evaluated based on the kinetic energy transferred on the wall. Specifically

1. A thermodynamically consistent one dimensional small strain model and a corresponding two dimensional model will be used to simulate the response of the multilayered polymer when subjected to impact.

2. A thermodynamically consistent three dimensional finite strain model will used used to simulate the impact response involving large deformation of the polymer

3.1 Scope

In the one dimensional study, a large layered plate which is infinite in the y and z directions and extends between 0 and l in the x direction was considered. In the two dimensional study a layered plate which is infinite in the z direction and extends between 0 and l in the x direction and extends between 0 and h in the y direction was considered. For the finite strain three dimensional model, finite dimensions in all three directions was considered. In all the studies carried out here, one face of the plate is beside a rigid surface while the impact is made on the opposite face. The interface regions are assumed to be fully bonded. The fragmentation of material when impacted is beyond the scope of this study. The creep compliance and

relaxation data which will be used to estimate the material parameters are obtained from the literature. The model used here is a specialization of the three dimensional framework developed by [30] where the thermal phenomena is suppressed.

3.2 Structure of the dissertation

The structure of the dissertation is as follows:

- Chapter 1 and 2 presents the research topic, with relevant literature survey and background information on the evolution of the impact resistant materials, models and experiments carried out to evaluate the performance of these materials.
- Chapter 3 discusses about the objective and the scope of this dissertation.
- In chapter 4, we use a small strain non linear model to study the response of the multilayered polymer subjected to impact using the finite volume numerical scheme. One dimensional and two dimensional models are considered to evaluate the performance of six different protocols.
- In chapter 5, we use a finite deformation model to study the behavior of layered plate when subjected to impact.
- We close in Chapter 6 with some final remarks on the different aspects of the work in this dissertation, and a discussion on future research directions.

4. SMALL STRAIN MODEL*

This chapter involves the development of the small strain model for the impact response of the layered polymer. As discussed in [28], when the rotations are small, upto strains of nearly 30% it is sufficient to consider only linearized kinematics, even though the constitutive equations are nonlinear. Therefore, we study the impact response of layered polymer using small strain model.

4.1 Governing equations

The conservation of linear momentum, in the absence of body forces reduces to

$$\rho \frac{\partial \hat{\mathbf{v}}}{\partial \hat{t}} = \hat{\mathrm{div}} \hat{\mathbf{T}} \tag{4.1}$$

where 'ρ' is the density of the material, '$\hat{\mathbf{v}}$' is the velocity and '$\hat{\mathbf{T}}$' stress tensor.

The two network theory[30] is used in this study to capture two basic phenomena of polymers when subjected to a constant load, i.e., instantaneous elasticity and delayed creep. This model consists of a temporary elastic network and a permanent backbone network. The former takes into account instantaneous elasticity and the latter takes into account the non-linear delayed creep response.

The total stress ($\hat{\mathbf{T}}$) on the network is the sum of the partial stresses $\hat{\mathbf{T}}^{(1)}$ and

* Reprint with permission from P. Alagappan, K. R. Rajagopal and A. R. Srinivasa, "Wave propagation due to impact through layered polymer composites", *Composite Structures*, Vol.115, pp.1-11, Copyright [2014] by Elsevier Limited

Reprint with permission from P. Alagappan, K. R. Rajagopal and A. R. Srinivasa, "Wave propagation due to impact through layered polymer composites:Part 2 - Planar problems", *Composite Structures*, Vol.131, pp.356-365, Copyright [2015] by Elsevier Limited

$\hat{\mathbf{T}}^{(2)}$ in each network respectively, i.e.,

$$\hat{\mathbf{T}} = \hat{\mathbf{T}}^{(1)} + \hat{\mathbf{T}}^{(2)} \tag{4.2}$$

The instantaneous elastic response of the temporary network 1 is given by

$$\frac{\partial \hat{\mathbf{T}}^{(1)}}{\partial \hat{t}} = \mathfrak{C}\mathbf{D} \tag{4.3}$$

and the delayed creep response of the permanent network 2 is given by

$$\frac{\partial \hat{\mathbf{T}}^{(2)}}{\partial \hat{t}} = \mathfrak{M}\left(\mathbf{D} - \eta(|\hat{\mathbf{T}}^{(2)}|^n)\hat{\mathbf{T}}^{(2)}\right) \tag{4.4}$$

where $\mathbf{D}$ is the symmetric part of velocity gradient, η is the power viscosity coefficient, n is th power law coefficient, $\mathfrak{C}$ and $\mathfrak{M}$ are fourth order elasticity tensors. We note that the elastic response is provided in a non-standard fashion, that is in terms of the time rate of the stress and the time rate of the strain. It will be later shown that the nonlinear response of viscoelastic material is captured using the above model.

4.2 One dimensional model

Let us consider a region that is infinite in y and z directions and extends between 0 and l in the x direction. The axial displacement, velocity and stress at any point 'x' at time 't' are given by $u(x,t)$, $v(x,t)$ and $\sigma(x,t)$, respectively. If we restrict ourselves to one dimensional case, equation (4.1) is given by

$$\rho\frac{\partial v}{\partial t} = \frac{\partial \sigma}{\partial x}. \tag{4.5}$$

The velocity, axial strain and strain rate are given as $\frac{\partial u}{\partial t}$, $\frac{\partial u}{\partial x}$ and $\frac{\partial v}{\partial x}$, respectively.

Thus the total stress σ from the equation (4.2) is given by

$$\sigma = \sigma_1 + \sigma_2 \tag{4.6}$$

The mechanical response of the network 1 from equation (4.3) is given by

$$\frac{\partial \sigma_1}{\partial t} = E_1 \dot{\epsilon} \tag{4.7}$$

The mechanical response of the network 2 from equation (4.4) is given by

$$\frac{\partial \sigma_2}{\partial t} = E_2 \dot{\epsilon} - \eta \sigma_2^n \tag{4.8}$$

where E_1 and E_2 are the elastic moduli and η is a power law viscosity coefficient and n is a power law coefficient. The nonlinearity in the response is evident in equation (4.8).

4.2.1 Non dimensionalization

Before using the finite volume technique to solve the momentum and constitutive equations it is necessary to choose appropriate scales to non dimensionalise them. The main reason for the non dimensionalization is to reduce the number of independent parameters so that we could assess the factors influencing the solution. Hence the equation (4.5), (4.7) and (4.8) are non-dimensionalised using characteristic length 'l_0' and characteristic time 't_0' which is the time taken by the wave to travel a distance 'l_0' in a material of modulus 'E' and density 'ρ'. Hence the characteristic scales used here are $u = l_0\bar{u}$, $v = v_0\bar{v}$, $\sigma = E\bar{\sigma}$, $t = t_0\bar{t}$, where $t_0 = l_0\sqrt{\frac{\rho}{E}}$.

$$\frac{L_0}{t_0}\frac{\partial \bar{u}}{\partial \bar{t}} = v_0 \bar{v}(\bar{x}, \bar{t}) \tag{4.9}$$

From equation (4.5)

$$\rho \frac{v_0}{t_0} \frac{\partial \bar{v}}{\partial \bar{t}} = \frac{E}{L_0} \frac{\partial \bar{\sigma}}{\partial \bar{x}}$$

Rearranging the above equation results in

$$\frac{\partial \bar{v}}{\partial \bar{t}} = \frac{E t_0}{L_0 \rho v_0} \frac{\partial \bar{\sigma}}{\partial \bar{x}}$$

Now let,

$$\frac{E t_0}{L_0 \rho v_0} = 1 \tag{4.10}$$

Hence, we can conclude from equation (4.9) and (4.10) that the characteristic time is

$$t_0 = L_0 \sqrt{\frac{\rho}{E}} \tag{4.11}$$

Therefore, the final non-dimensionalized equations are

$$\frac{d\bar{v}}{d\bar{t}} = \frac{d\bar{\sigma}}{d\bar{x}} \tag{4.12}$$

$$\bar{\sigma} = \bar{\sigma}_1 + \bar{\sigma}_2 \tag{4.13}$$

$$\frac{d\bar{\sigma}_1}{d\bar{t}} = \gamma \frac{d\bar{v}}{d\bar{x}} \tag{4.14}$$

$$\frac{d\bar{\sigma}_2}{d\bar{t}} = \alpha \frac{d\bar{v}}{d\bar{x}} - \beta \bar{\sigma}_2^n \tag{4.15}$$

where $\alpha = \frac{E_2}{E}$, $\beta = \eta t_0 E^{n-1}$, $\gamma = \frac{E_1}{E}$ and $E = E_1 + E_2$.

The parameters α , β and γ depends upon the type of material. The equations are solved using finite volume method.

4.2.2 Material parameter

The creep compliance data for PC and PU used in this study for calculating the material parameters were obtained from Jazouli et al. [21] and Yao et al. [39] respectively. The PC creep experiment was conducted at room temperature for 3600 seconds at constant stress of 46.3 MPa. The PU creep experiment was conducted at a temperature of 30°C for 560 seconds at constant stress of 2.5 MPa. The parameters obtained are shown in Table 4.1. A comparison of the predictions from the solution of the model versus the experimental results for PC and PU are depicted in Figure 4.8 and 4.9 respectively. Surprisingly, such a simple power law nonlinearity is sufficient to represent very well the very slow decay of response that is observed in polymeric materials. This is in contrast to linear Prony series models where many relaxation times need to be used to capture this phenomenon.

Table 4.1: Material parameters for the one dimensional model based on creep compliance data

	PC	PU
α	1.404	0.784
β	0.1324	2.486
γ	0.0887	0.216

4.2.3 Solution technique

The FVM involves the discretization of the domain into number of non-overlapping control volumes(the region between dotted lines in figure 4.1). For each control vol-

ume, the conservation form of the equation of momentum is given by

$$\int_{V^i} \rho \frac{\partial \mathbf{v}}{\partial t} dV^i = \int_{\Omega^i} \sigma \bullet \mathbf{n} d\Omega^i \tag{4.16}$$

where V^i is the discrete control volume, $d\Omega^i$ is the boundary surface of V^i and $\mathbf{n}$ is the outward pointing unit normal along the boundary surface $d\Omega^i$.

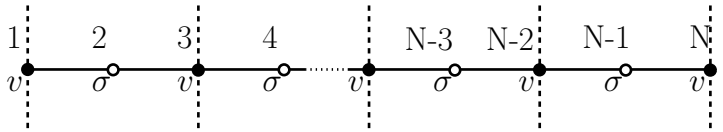

Figure 4.1: 1d grid representation showing the stress control volume and the location of the stress and velocity nodes

4.2.4 Analytical solution for the standard linear solid model

When the power law coefficient in the equation (4.8) is equal to 1, the model reduces to a standard linear solid model [38]. This provides us a way to test the convergence and accuracy of the scheme by comparing it with the analytical solution. To be specific, if the power law coefficient is set to be 1 we obtain

$$\frac{d\bar{\sigma}_2}{d\bar{t}} = \alpha \frac{d\bar{v}}{d\bar{x}} - \beta \bar{\sigma}_2 \tag{4.17}$$

If we assume that the initial velocity is sinusoidal

$$v(x, 0) = sin(\frac{\pi x}{L})$$

Then, the linearity of the differential equation will imply that the spatial variation of the velocity will also be sinusoidal. Therefore, velocity field is given by

$$v(x,t) = \bar{v}(t) sin(\frac{\pi x}{L})$$

Since the stress is linear in the spatial derivative of the velocity, it will be cosine in nature. Therefore, the stress in network 1 is given by

$$\sigma_1(x,t) = \bar{\sigma}_1(t) cos(\frac{\pi x}{L})$$

and the stress in network 2 is given by

$$\sigma_2(x,t) = \bar{\sigma}_2(t) cos(\frac{\pi x}{L})$$

Substituting the above results in equation (4.12) gives

$$\begin{aligned} sin(\frac{\pi x}{L})\frac{d\bar{v}(t)}{dt} &= \bar{\sigma}_1(t)\frac{\pi}{L}(-sin(\frac{\pi x}{L})) + \bar{\sigma}_2(t)\frac{\pi}{L}(-sin(\frac{\pi x}{L})); \\ \Rightarrow \frac{d\bar{v}(t)}{dt} &= -\frac{\pi}{L}\bar{\sigma}_1(t) - \frac{\pi}{L}\bar{\sigma}_2(t) \\ \Rightarrow \frac{d\bar{v}(t)}{dt} &= -\frac{\pi}{L}(\bar{\sigma}_1(t) + \bar{\sigma}_2(t)) \end{aligned}$$

Substituting the results in equation (4.14) gives

$$\begin{aligned} cos(\frac{\pi x}{L})\frac{d\bar{\sigma}_1(t)}{dt} &= \gamma\bar{v}(t)\frac{\pi}{L}cos(\frac{\pi x}{L}); \\ \Rightarrow \frac{d\bar{\sigma}_1(t)}{dt} &= \gamma\bar{v}(t)\frac{\pi}{L}; \end{aligned}$$

Substituting the results in equation (4.15) gives

$$\begin{aligned} cos(\frac{\pi x}{L})\frac{d\bar{\sigma_2}(t)}{dt} &= \alpha\bar{v}(t)\frac{\pi}{L}cos(\frac{\pi x}{L}) - \beta\bar{\sigma}_2(t)cos(\frac{\pi x}{L}); \\ \Rightarrow \frac{d\bar{\sigma_2}(t)}{dt} &= \alpha\bar{v}(t)\frac{\pi}{L} - \beta\bar{\sigma}_2(t) \end{aligned}$$

The equilibrium and constitutive equation can be written in the matrix form as

$$\begin{bmatrix} \frac{d\bar{\sigma}_1(t)}{dt} \\ \frac{d\bar{\sigma}_2(t)}{dt} \\ \frac{d\bar{v}(t)}{dt} \end{bmatrix} = \begin{bmatrix} 0 & 0 & \frac{\gamma\pi}{L} \\ 0 & -\beta & \frac{\alpha\pi}{L} \\ -\frac{\pi}{L} & -\frac{\pi}{L} & 0 \end{bmatrix} \begin{bmatrix} \bar{\sigma}_1(t) \\ \bar{\sigma}_2(t) \\ \bar{v}(t) \end{bmatrix} \tag{4.18}$$

The above equation is of the form

$$\frac{d\boldsymbol{X}(t)}{dt} = \boldsymbol{A}\boldsymbol{x}(t)$$

where $\boldsymbol{X}(t) = \begin{bmatrix} \bar{\sigma}_1(t) \\ \bar{\sigma}_2(t) \\ \bar{v}(t) \end{bmatrix}$ and $\boldsymbol{A} = \begin{bmatrix} 0 & 0 & \frac{\gamma\pi}{L} \\ 0 & -\beta & \frac{\alpha\pi}{L} \\ -\frac{\pi}{L} & -\frac{\pi}{L} & 0 \end{bmatrix}$.

Solving the above first order ODE results in

$$\boldsymbol{X}(t) = \boldsymbol{X}(0)exp(\boldsymbol{A}t) \tag{4.19}$$

The figure 4.2 shows the comparison of analytical solution of the stress in the wall for a time period of 100 units with the FVM numerical scheme. It can be seen that both the results agree exceptionally well.

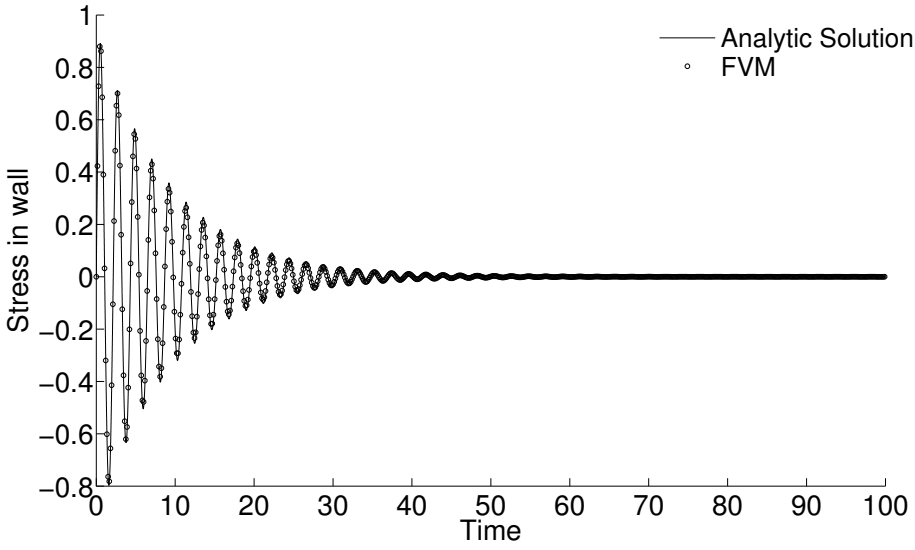

Figure 4.2: Comparison of analytical and numerical solutions for the standard linear solid model. This is used to verify the accuracy of the numerical scheme.

4.2.5 Problem description

We consider six different material combinations 1. pure PC, 2. pure PU, 3. bilayer(PU/PC), 4. bilayer(PC/PU) 5. trilayer(PC/PU/PC) and 6. trilayer(PU/PC/PU). In order to carry out a simulation of the impact response in each of these six cases, one face of the plate is fixed while the other face is given a ramp stress with slope 'a' for a time 't_0' and is maintained constant until 't_1' and decreased to '0' and held constant(see figure 4.3). Thus the initial condition is

$$u(x,t) = 0, \quad v(x,t) = 0 \quad \forall t <= 0. \tag{4.20}$$

The boundary conditions are

$$\sigma(0,t) = 0 \forall t > 0. \tag{4.21}$$

and at $\sigma(l,t)$, it is as shown in figure 4.3 $\forall t > 0$.

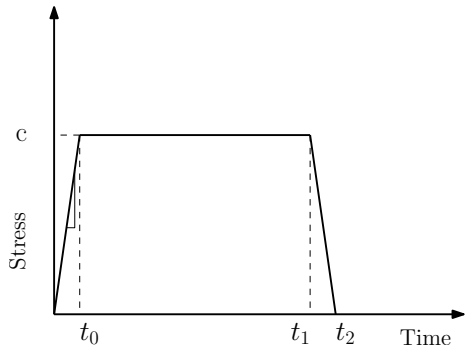

Figure 4.3: Initial condition

4.2.6 Results and discussion

The important application of interest with regard to the layered polymer that is used here, is to reduce the impact on the wall besides which it is in contact. The figures 4.4 and 4.5 shows the kinetic energy on the wall when PU and PC is impacted respectively. The peaks in figures represent the time when the impact wave reaches the wall. Two extreme types of behavior are observed when using a pure PC layer and pure PU layer i.e., the time taken for the wave to reach the wall in the former material is 1 unit of time while in case of latter material it is 2 units of time. Time taken for the wave to reach the wall in the bilayer (PU/PC) and the bilayer (PC/PU) is around 1.5 units, in case of the trilayer (PU/PC/PU) and the trilayer (PC/PU/PC), it is 1.6 and 1.4 units respectively. The most important aspects that needs to be taken into account in the designing of polymer composites as shock absorbers is the magnitude of the kinetic energy on the wall. From the one dimensional study conducted the kinetic energy on the wall in ascending order

is as follows PC/PU/PC, pure PC, PC/PU, PU/PC/PU, PU/PC and pure PU. It should be noted that the performance of a trilayer is always not better bilayer and individual layers. The magnitude of the kinetic energy is lowest in case of the trilayer (PC/PU/PC) with regard to the six different layers that were considered. This trilayer combination has a compliant layer between two stiff layers.

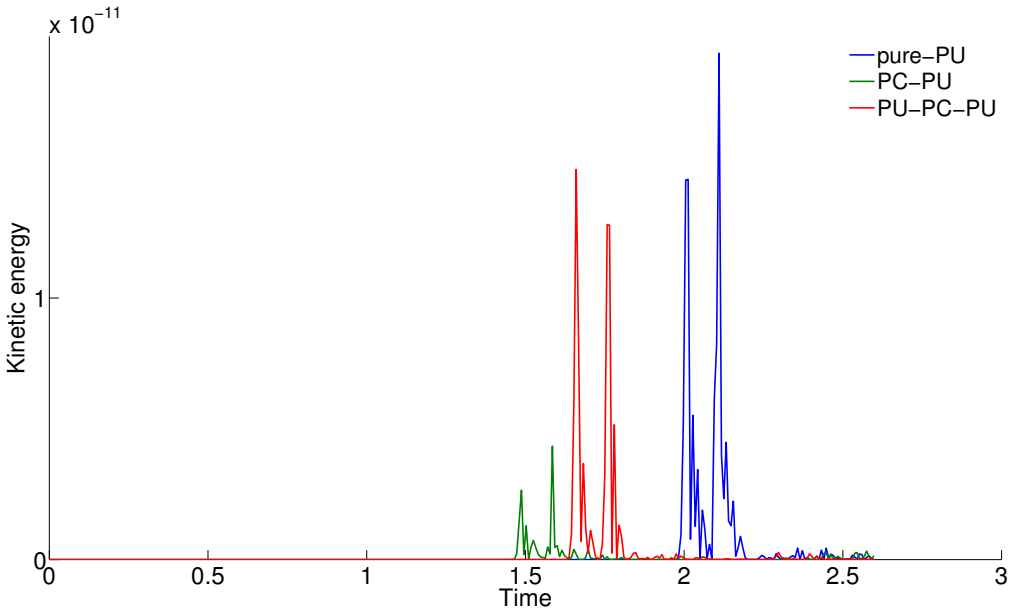

Figure 4.4: Kinetic energy at the wall when PU is impacted

4.3 Two dimensional model

Let us consider a plate, which is infinite in the z direction and has finite dimensions in x and y direction (see Figure 4.6). The stress tensor, displacement vector and velocity vector at any time '$\hat{t}$' in the domain are represented by $\hat{\mathbf{T}}$(x,y,$\hat{t}$), $\hat{\mathbf{d}}$(x,y,$\hat{t}$) and $\hat{\mathbf{v}}$(x,y,$\hat{t}$), respectively.

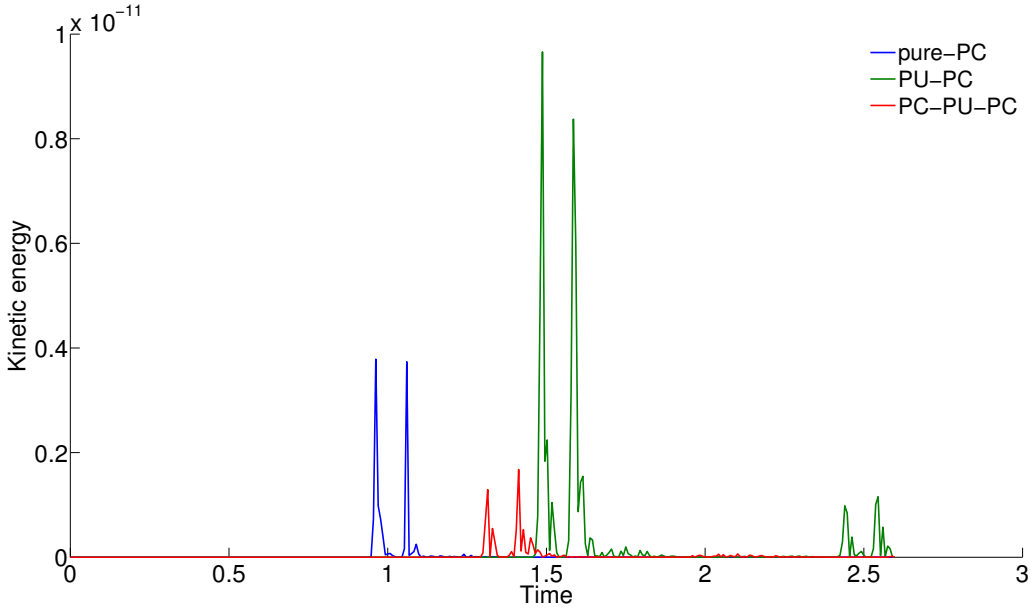

Figure 4.5: Kinetic energy at the wall when PC is impacted

If we restrict ourselves to two dimensions from equation (4.1) we have,

$$\rho\frac{\partial\hat{v}_1}{\partial\hat{t}} = \frac{\partial\hat{T}_{xx}}{\partial\hat{x}} + \frac{\partial\hat{T}_{xy}}{\partial\hat{y}} \tag{4.22}$$

$$\rho\frac{\partial\hat{v}_2}{\partial\hat{t}} = \frac{\partial\hat{T}_{xy}}{\partial\hat{x}} + \frac{\partial\hat{T}_{yy}}{\partial\hat{y}} \tag{4.23}$$

4.3.1 Non dimensionalization

Nondimensionalization is done using the characteristic scales $\hat{\mathbf{v}} = v_0\mathbf{v}$,$\hat{\mathbf{T}} = G\mathbf{T}$, $\hat{t} = t_0 t$, $\hat{x} = l_0 x$ and $\hat{y} = l_0 y$. Using the characteristic scales, equation (4.22) leads to

$$\frac{\rho v_0 l_0}{t_0 G}\frac{\partial v_1}{\partial t} = \frac{\partial T_{xx}}{\partial x} + \frac{\partial T_{xy}}{\partial y} \tag{4.24}$$

If we consider t_0 to be the time taken by the wave to travel a distance l_0 through the material which has a modulus G(this is the Young's modulus one obtains when

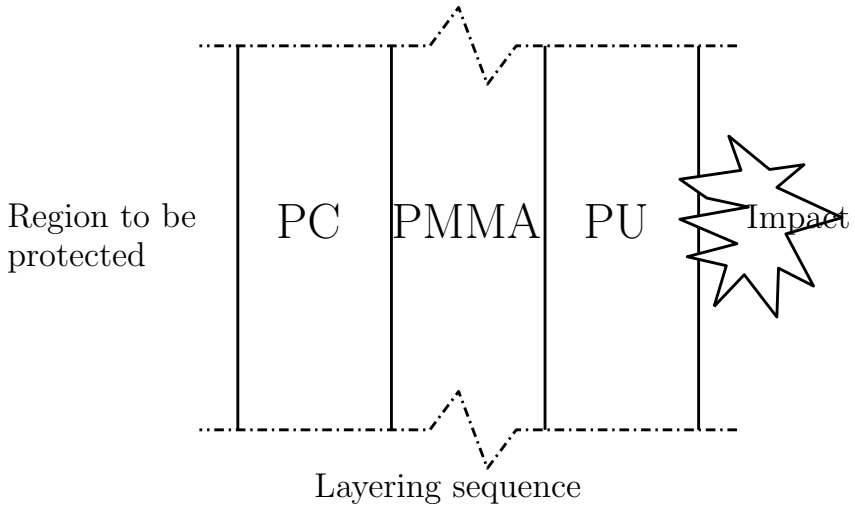

Figure 4.6: Schematic representation of impact

one linearizes the elastic response) and density ρ, then $t_0 = l_0\sqrt{\rho/G}$ and the above equation reduces to

$$\frac{\partial v_1}{\partial t} = \frac{\partial T_{xx}}{\partial x} + \frac{\partial T_{xy}}{\partial y} \tag{4.25}$$

Similarly, non dimensionalizing 'y' momentum equation we have

$$\frac{\partial v_2}{\partial t} = \frac{\partial T_{xy}}{\partial x} + \frac{\partial T_{yy}}{\partial y} \tag{4.26}$$

The nondimensionlized constitutive equation for the two dimensional problem

from equations (4.3) and (4.4) is given by

$$\begin{bmatrix} \frac{\partial T_{xx}^{(1)}}{\partial t} \\ \frac{\partial T_{yy}^{(1)}}{\partial t} \\ \frac{\partial T_{xy}^{(1)}}{\partial t} \end{bmatrix} = \alpha \begin{bmatrix} 1-\nu & \nu & 0 \\ \nu & 1-\nu & 0 \\ 0 & 0 & \frac{1-2\nu}{2} \end{bmatrix} \begin{bmatrix} \frac{\partial u}{\partial x} \\ \frac{\partial v}{\partial y} \\ \left(\frac{\partial u}{\partial y} + \frac{\partial v}{\partial x}\right) \end{bmatrix} \tag{4.27}$$

where $\alpha = \frac{E_1}{G(1+\nu)(1-2\nu)}$ and $G = E_1 + E_2$.

$$\begin{bmatrix} \frac{\partial T_{xx}^{(2)}}{\partial t} \\ \frac{\partial T_{yy}^{(2)}}{\partial t} \\ \frac{\partial T_{xy}^{(2)}}{\partial t} \end{bmatrix} = \beta \begin{bmatrix} 1-\nu & \nu & 0 \\ \nu & 1-\nu & 0 \\ 0 & 0 & \frac{1-2\nu}{2} \end{bmatrix} \begin{bmatrix} \frac{\partial u}{\partial x} \\ \frac{\partial v}{\partial y} \\ \frac{1}{2}\left(\frac{\partial u}{\partial y} + \frac{\partial v}{\partial x}\right) \end{bmatrix} - \gamma A \begin{bmatrix} 1-\nu & \nu & 0 \\ \nu & 1-\nu & 0 \\ 0 & 0 & \frac{1-2\nu}{2} \end{bmatrix} \begin{bmatrix} T_{xx}^{(2)} \\ T_{yy}^{(2)} \\ T_{xy}^{(2)} \end{bmatrix} \tag{4.28}$$

where $\beta = \frac{E_2}{G(1+\nu)(1-2\nu)}$, $\gamma = \frac{G^3\eta}{G(1+\nu)(1-2\nu)}$ and $A = (T_{xx}^{(2)})^2 + (T_{yy}^{(2)})^2 + 2 * (T_{xy}^{(2)})^2$

Integrating the momentum equation in the x-direction over the discrete velocity control volume V_P (see dashed control volume in figure 4.7), we obtain

$$\int_{CV} \frac{\partial u}{\partial t} dV_P = \int_{CV} \left(\frac{\partial T_{xx}}{\partial x} + \frac{\partial T_{xy}}{\partial y} \right) dV_P \tag{4.29}$$

$$\frac{\partial u}{\partial t} \Delta x \Delta y = \left(Txx|_E - Txx|_W\right) \Delta y + \left(Txy|_N - Txy|_S\right) \Delta x \tag{4.30}$$

Similarly the momentum equation in the y-direction is also integrated over the control volume. The velocity gradients in the constitutive equation are approximated using central difference formula with equal weightage for the nodes on the either side.

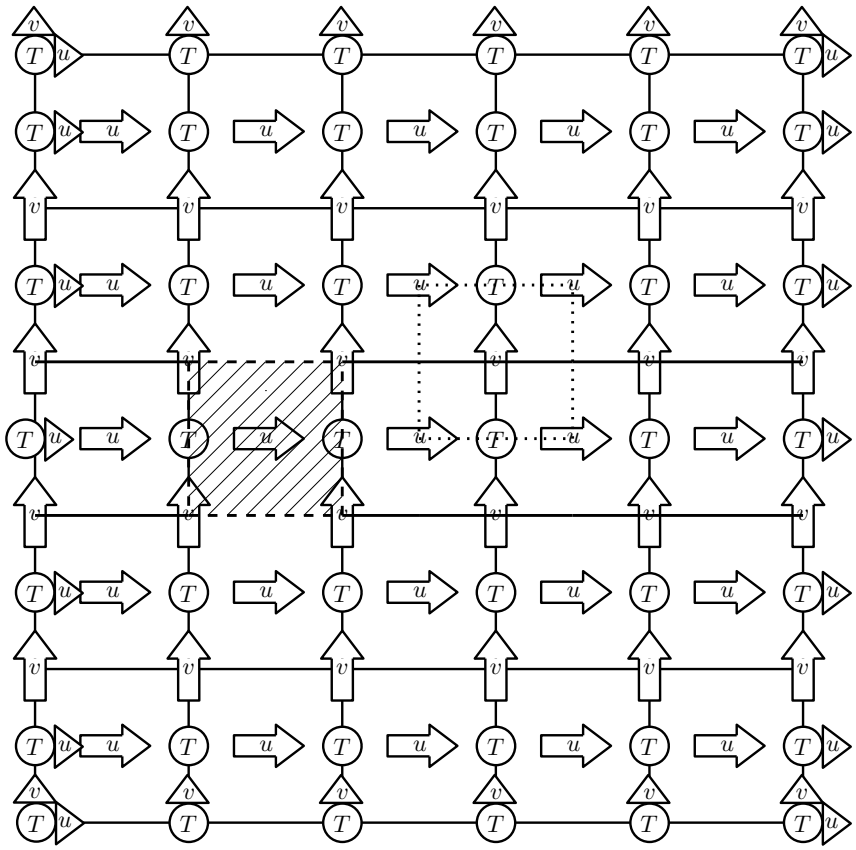

Figure 4.7: A representation of staggered grid used in this study. T is the stress, u and v are the x and y component of velocity respectively. A sample u and v control volume is represented by the cross hatched and dotted line region respectively. The u control volume at the left and the right face of the plate is half the cross hatched region and similarly v control volume at the top and bottom of the plate is half the dotted region.

The final discretized equations are

$$
\begin{aligned}
u_P^{k+1} &= u_P^k + \frac{\Delta t}{\Delta x}\left(T_{xxE}^k - T_{xxW}^k\right) + \frac{\Delta t}{\Delta y}\left(T_{xyN}^k - T_{xyS}^k\right) \\
v_P^{k+1} &= v_P^k + \frac{\Delta t}{\Delta x}\left(T_{xyE}^k - T_{xyW}^k\right) + \frac{\Delta t}{\Delta y}\left(T_{yyN}^k - T_{yyS}^k\right) \\
T_{xxP}^{(1)k+1} &= T_{xxP}^{(1)k} + \alpha\Delta t\left(\left(\frac{u_E^k - u_W^k}{\Delta x}\right) + \nu\left(\frac{v_N^k - v_S^k}{\Delta y}\right)\right) \\
T_{yyP}^{(1)k+1} &= T_{yyP}^{(1)k} + \alpha\Delta t\left(\nu\left(\frac{u_E^k - u_W^k}{\Delta x}\right) + \left(\frac{v_N^k - v_S^k}{\Delta y}\right)\right) \\
T_{xyP}^{(1)k+1} &= T_{xyP}^{(1)k} + \alpha\Delta t\frac{1-\nu}{2}\left(\frac{1}{\Delta y}\left(u_N^k - u_S^k\right) + \left(v_E^k - v_W^k\right)\frac{1}{\Delta x}\right) \\
T_{xxP}^{(2)k+1} &= T_{xxP}^{(2)k} + \beta\Delta t\left(\left(\frac{u_E^k - u_W^k}{\Delta x}\right) + \nu\left(\frac{v_N^k - v_S^k}{\Delta y}\right)\right) - \gamma\Delta t A_P^k\left(T_{xxP}^{(2)k} + \nu T_{xyP}^{(2)k}\right) \\
T_{yyP}^{(2)k+1} &= T_{yyP}^{(2)k} + \beta\Delta t\left(\nu\left(\frac{u_E^k - u_W^k}{\Delta x}\right) + \left(\frac{v_N^k - v_S^k}{\Delta y}\right)\right) - \gamma\Delta t A_P^k\left(\nu T_{xxP}^{(2)k} + T_{xyP}^{(2)k}\right) \\
T_{xyP}^{(2)k+1} &= T_{xyP}^{(2)k} + \beta\Delta t\frac{1-\nu}{2}\left(\frac{1}{\Delta y}\left(u_N^k - u_S^k\right) + \left(v_E^k - v_W^k\right)\frac{1}{\Delta x}\right) - \gamma\Delta t\frac{1-\nu}{2}T_{xyP}^{(2)k}A_P^k
\end{aligned}
$$

where $A_P = ((T_{xxP}^{(2)})^2 + (T_{yyP}^{(2)})^2 + 2(T_{xyP}^{(2)})^2)$. The points E, W, N and S represents the east, west, north and south direction for the control volume respectively and P is the point of interest in the control volume. The material parameters are α, β and γ. Δt, Δx , Δy and k represents the time, space discretization in x and y direction and time step respectively .

4.3.2 Material parameter

The PC and PU experimental data used in the one dimensional model is used for the two dimensional analysis(see table 4.2 for the material parameters). The Poissson's ratio for PU and PC are obtained from Jain et al. [20] and Shah [31].

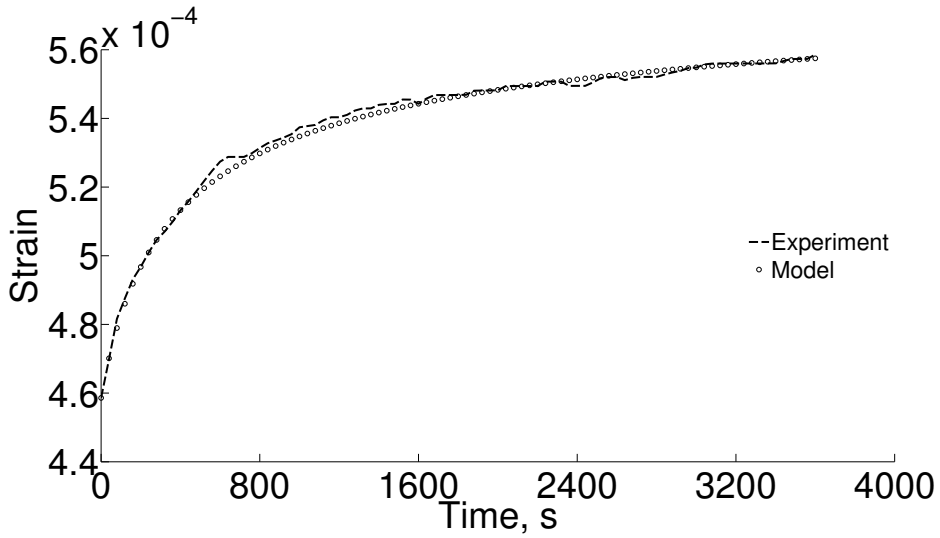

Figure 4.8: Experiments for PC [21] compared with the prediction of the implicit model presented here. Notice the good match for the nonlinear creep compliance based on the constitutive parameters given in equations (4.27) and (4.28).

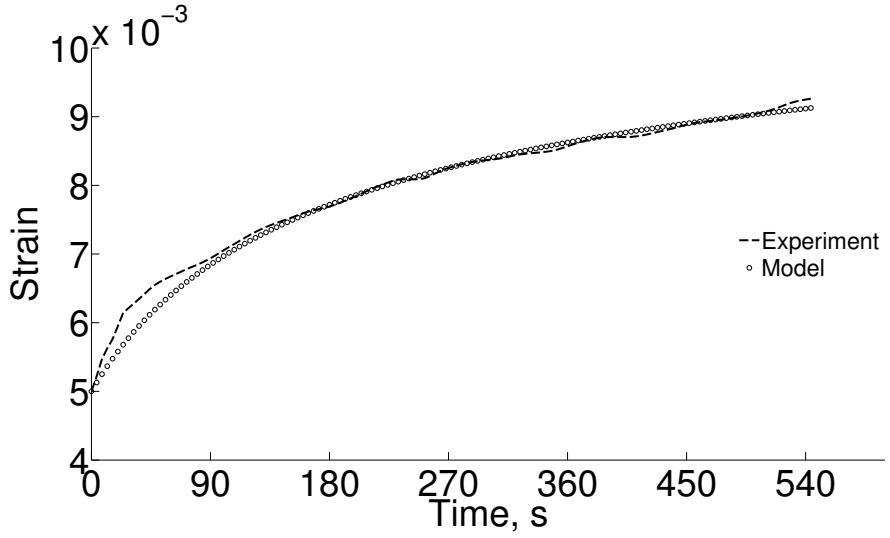

Figure 4.9: Experiments for PU [39] compared with the prediction of the implicit model presented here. Notice the good match for the nonlinear creep compliance based on the constitutive parameters given in equations (4.27) and (4.28).

Table 4.2: Material parameters for the two dimensional model based on creep compliance data

	PC	PU
α	1.5037	0.1854
β	0.4194	0.2555
γ	2.9521	0.2240
ν	0.37 [31]	0.477 [20]

4.3.3 Cross validation of numerical result

Similar to the one dimensional model, when the viscous response in the network is linear, the model reduces to a standard linear solid model. This provides us with a way to test the accuracy of the scheme when compared to the numerical solution of the ODE's.

Let us consider a plate of thickness 'L' and height 'H'. If we assume that the initial 'x' and 'y' components of velocity to be sine and cosine respectively, i.e.

$$\bar{u}(x,y,0) = sin\left(\frac{\pi x}{L}\right) sin\left(\frac{\pi y}{H}\right); \quad \bar{v}(x,y,0) = cos\left(\frac{\pi x}{L}\right) cos\left(\frac{\pi y}{H}\right) \tag{4.31}$$

then the velocity and stress are given by

$$\begin{aligned}
\bar{u}(x,y,t) &= u(t) sin\left(\frac{\pi x}{L}\right) sin\left(\frac{\pi y}{H}\right); \bar{v}(x,y,t) = v(t) cos\left(\frac{\pi x}{L}\right) cos\left(\frac{\pi y}{H}\right); \\
\bar{T}_{xx}(x,y,t) &= T_{xx}(t) cos\left(\frac{\pi x}{L}\right) sin\left(\frac{\pi y}{H}\right); \bar{T}_{yy}(x,y,t) = T_{yy}(t) cos\left(\frac{\pi x}{L}\right) sin\left(\frac{\pi y}{H}\right); and \\
\bar{T}_{xy}(x,y,t) &= T_{xy}(t) sin\left(\frac{\pi x}{L}\right) cos\left(\frac{\pi y}{H}\right)
\end{aligned}$$

The final ordinary differential equations are

$$\begin{bmatrix} \frac{\partial u}{\partial t} \\ \\ \frac{\partial v}{\partial t} \end{bmatrix} = \begin{bmatrix} -\frac{\pi}{L}T_{xx}(t) - \frac{\pi}{H}T_{xy}(t) \\ \\ \frac{\pi}{L}T_{xy}(t) + \frac{\pi}{H}T_{yy}(t) \end{bmatrix}$$

$$\begin{bmatrix} \frac{\partial T_{xx}^{(1)}}{\partial t} \\ \\ \frac{\partial T_{yy}^{(1)}}{\partial t} \\ \\ \frac{\partial T_{xy}^{(1)}}{\partial t} \end{bmatrix} = \alpha \begin{bmatrix} (1-\nu)u(t)\frac{\pi}{L} - \nu v(t)\frac{\pi}{H} \\ \\ \nu u(t)\frac{\pi}{L} - (1-\nu)\frac{\pi}{H} \\ \\ \frac{1-2\nu}{2}\left(u(t)\frac{\pi}{H} - v(t)\frac{\pi}{L}\right) \end{bmatrix}$$

$$\begin{bmatrix} \frac{\partial T_{xx}^{(2)}}{\partial t} \\ \\ \frac{\partial T_{yy}^{(2)}}{\partial t} \\ \\ \frac{\partial T_{xy}^{(2)}}{\partial t} \end{bmatrix} = \beta \begin{bmatrix} (1-\nu)u(t)\frac{\pi}{L} - \nu v(t)\frac{\pi}{H} \\ \\ \nu u(t)\frac{\pi}{L} - (1-\nu)\frac{\pi}{H} \\ \\ \frac{1-2\nu}{2}\left(u(t)\frac{\pi}{H} - v(t)\frac{\pi}{L}\right) \end{bmatrix} - \gamma \begin{bmatrix} (1-\nu)T_{xx}^{(2)}(t) + \nu T_{yy}^{(2)}(t) \\ \\ \nu T_{xx}^{(2)}(t) + (1-\nu)T_{yy}^{(2)}(t) \\ \\ \frac{1-2\nu}{2}T_{xy}^{(2)}(t) \end{bmatrix}$$

The above equations are solved using finite volume technique and MATLAB® ODE solver. The resulting 'x' component of velocity at the center of the domain predicted by the model is compared with the solution of the ODE solver for a time period of 8.3 units and is shown in figure 4.10 and it can be seen both results agree exceptionally well.

4.3.4 Problem description

The impact on a rectangular plate of non dimensionalized thickness 'L' and height 'H' is simulated by applying stress in a localized region of height "$2b$"(see figure 4.11) on one face of the plate while the other face of the plate is fixed. The initial conditions

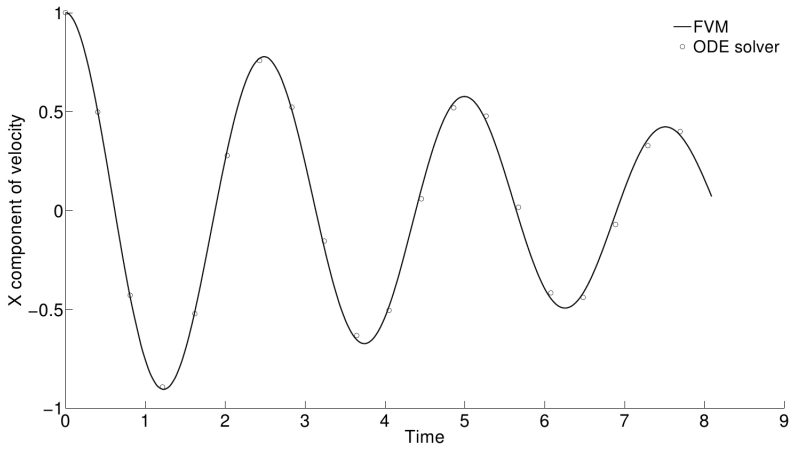

Figure 4.10: Comparison of the x component of velocity at the center of the domain obtained from FVM with MATLAB^{TM}ODE solver solution

are

$$\mathbf{T}(x, y, t) = 0, \quad u(x, y, t) = 0 \quad v(x, y, t) = 0 \quad \forall t <= 0. \tag{4.32}$$

.

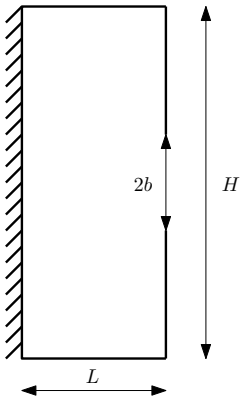

Figure 4.11: Rectangular plate of dimensions T x H, the impact region is of length '$2b$'.

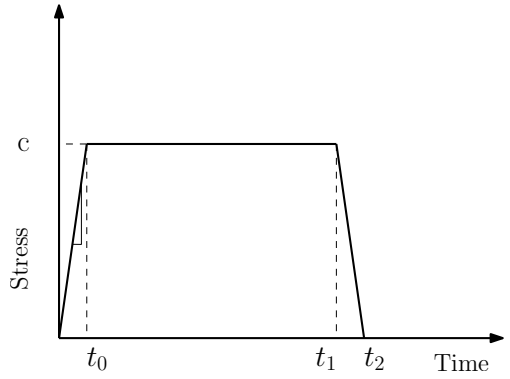

Figure 4.12: Temporal boundary condition for the impact region.

Figure 4.12 shows the boundary condition for the stress(T_{xx}) in the localized region of length '2b' on the impact face while the opposite face is fixed. The remaining region is assumed to be stress free. The performance of the six different protocols to the above boundary conditions considered in this study are evaluated by comparing the kinetic energy.

4.3.5 Results and discussions

Kinetic energy propagation in time

Figures 4.13 through 4.18 shows the nondimensionalized kinetic energy at different instants of time for the various cases considered in this study. The propagation of energy through the pure PC layer at different instants of time before and after impact from the wall is shown in figure 4.13. The propagation resembles that of a parabolic profile with higher intensity along the axis of impact and decreases away from it. The intensity of the wave dampens as it propagates through the domain. The figures 4.14 show the propagation through pure PU layer. In case of pure PC the wave has reflected from the wall whereas in pure PU layer it has just crossed the center of the domain. This is due to the lower stiffness of the pure PU when compared to that of pure PC layer. Similar to the pure PC the intensity of wave dampens as it propagates through the domain. The figures 4.15 and 4.16 show the energy propagation through the bilayer(PC/PU and PU/PC) when PU and PC are impacted at different instants of time each, respectively. In the bilayer it can be seen that waves gets partly reflected and partly transmitted at the interface in the center of the domain. As a result of the interaction the energy decreases by 54.19%(bilayer PC/PU) and 14.06%(bilayer PU/PC) when PU and PC are impacted, respectively. The amount of energy reduced is significantly higher when the wave propagates into a stiff layer from a compliant layer. The figures 4.17 and 4.18 show the propagation

through the trilayer(PC/PU/PC and PU/PC/PU) when PC and PU are impacted. The energy at the first interface(near wall) decreases by 75.50% and 12.13% whereas at the second interface(near impact side) it decreases by 29.04% and 62.96% when PC and PU is impacted respectively. The overall performance of the layered composite is analyzed based on the amount of energy transferred to the wall. The energy on the wall at different instants of time are shown in figures 4.19 and 4.20 when PU and PC are impacted, respectively. The peaks represent the arrival of the impact influence on the wall. Since the propagation velocity depends on the type of material, the time taken fot the impact to reach the wall is different for the different layering sequence. It can be seen from the figures 4.19 and 4.20 that bilayer PU/PC and PC/PU have the same arrival time at the wall whereas the magnitude of kinetic energy is different. From the two dimensional study conducted the magnitude of kinetic energy on the wall in ascending order is as follows PC/PU/PC, pure PC, PC/PU, PU/PC, PU/PC/PU and pure PU. When compared to the one dimensional results the performance of bilayer(PU/PC) and trilayer(PU/PC/PU) gets interchanged which is due to the interaction through the 2d domain. The overall better performance in terms of kinetic energy on the wall is trilayer(PC/PU/PC) which is the same result of as one dimensional study.

4.3.6 Conclusion

The performance of the two materials PC and PU under impact has been studied using a nonlinear rate type model and then studying the equations governing the response of the material numerically using a FVM approach. The parameters characterizing the model were obtained from the creep compliance data found in the literature. The reflected and the transmitted wave characteristics for the layered materials were studied using the model. The model used in this study captures the

reflection phenomenon due to the interaction of the waves at the interface. The comparison of the kinetic energy in the wall when using different combinations of PC and PU was carried out. The results show that the kinetic energy on the wall is lowest when using a composite layer with the PU/PC/PU structure. This method can be used to serve as a tool for selecting better impact resistant composite bodies subjected small strain deformation.

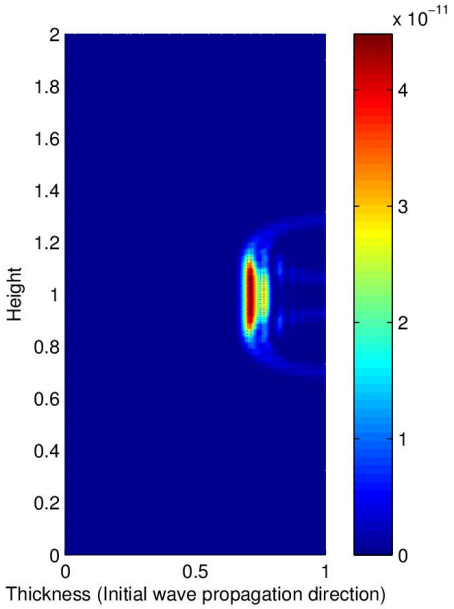

(a) At 0.3 units of time when PC is impacted. The parabolic profile of the wave propagation with high intensity at the center with decreasing intensity away from the center.

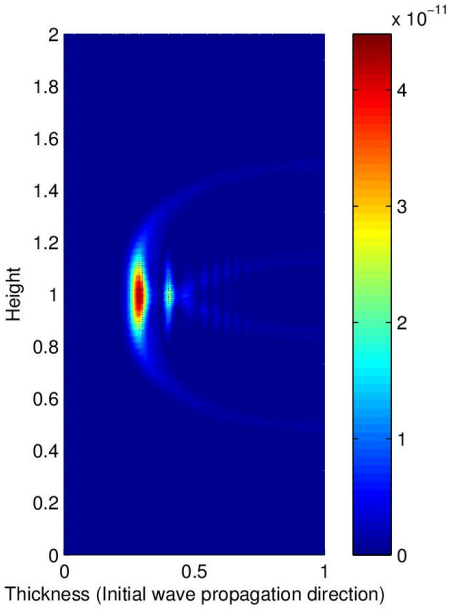

(b) At 0.65 units of time when PC is impacted.

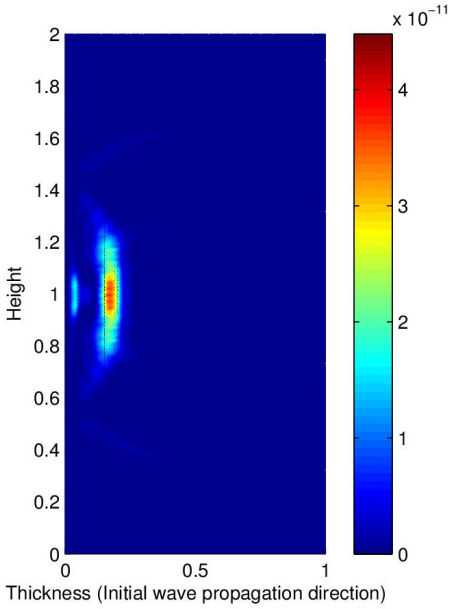

(c) At 1.0 units of time when PC is impacted. Reflection from the wall.

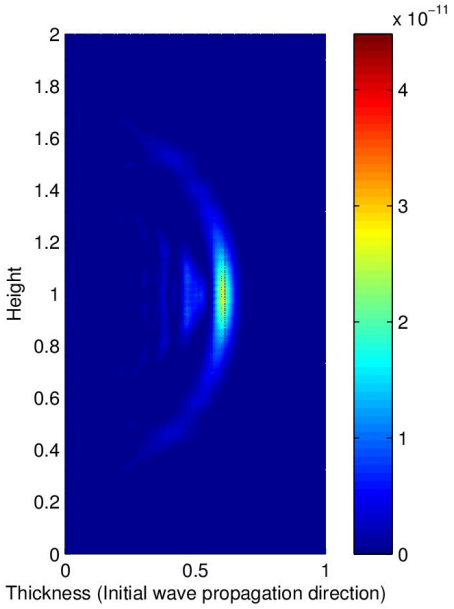

(d) At 1.4 units of time when PC is impacted. The amplitude of the energy has reduced.

Figure 4.13: Comparison of the nondimensionalized kinetic energy for PC at different instants of time

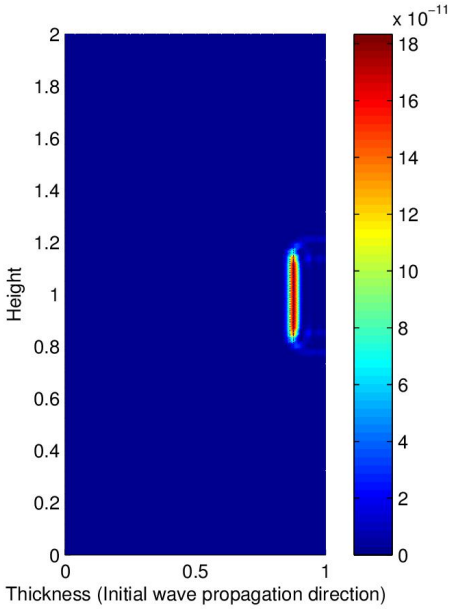

(a) At 0.3 units of time the wave has not reached the center of the domain. The profile is similar to that observed in PC layer.

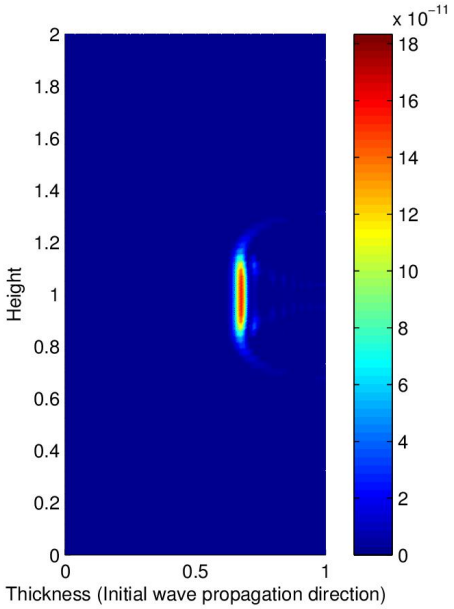

(b) The propagation through pure PU at 0.65 units of time.

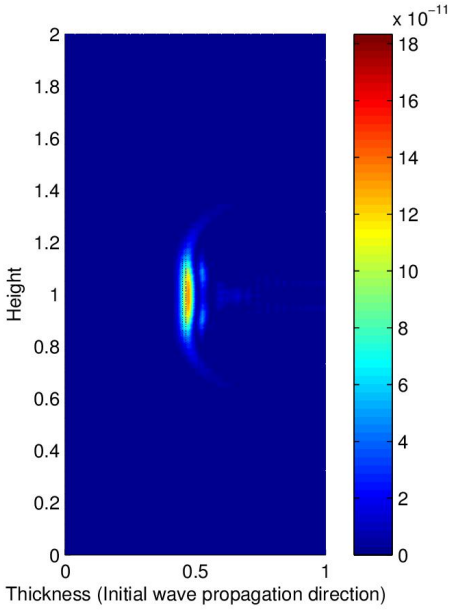

(c) At 1.0 units of time the wave has just crossed the center of the domain.

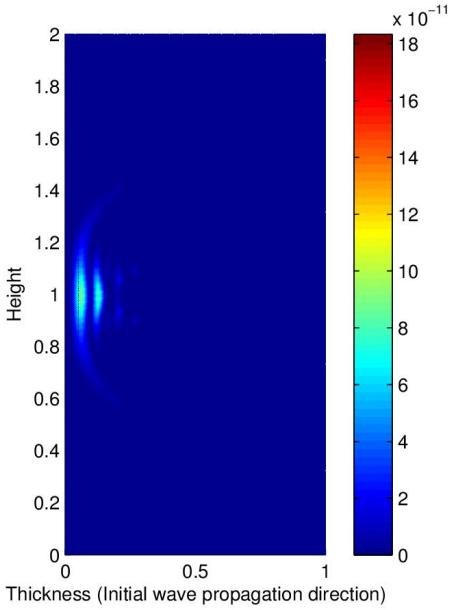

(d) At 1.8 units of time the wave has reached the opposite face of impact.

Figure 4.14: Comparison of the nondimensionalized kinetic energy for PU at different instants of time

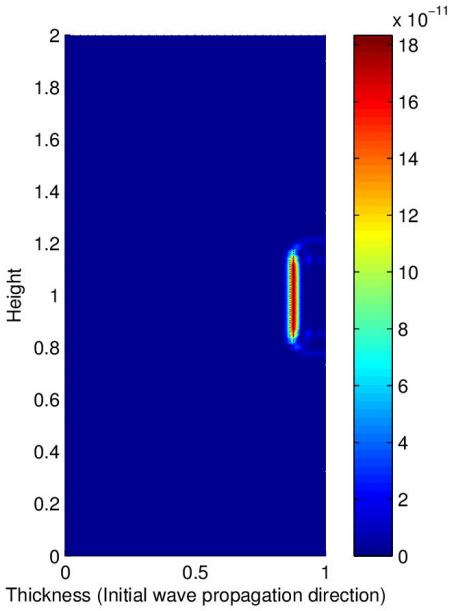

(a) At 0.3 units of time the propagation is through PU and hence it is similar to pure PU layer.

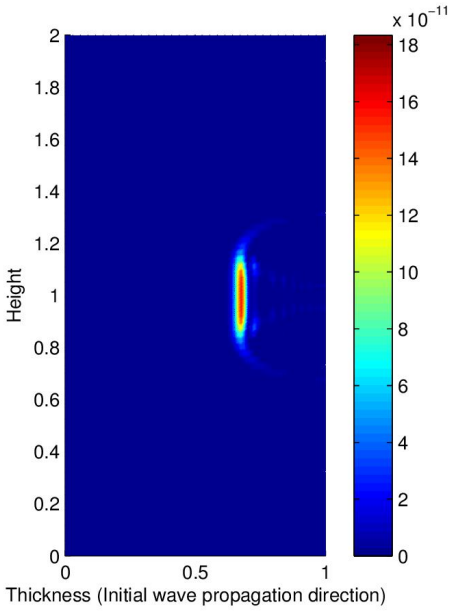

(b) At 0.65 units of time, same behavior as observed in pure PU layer.

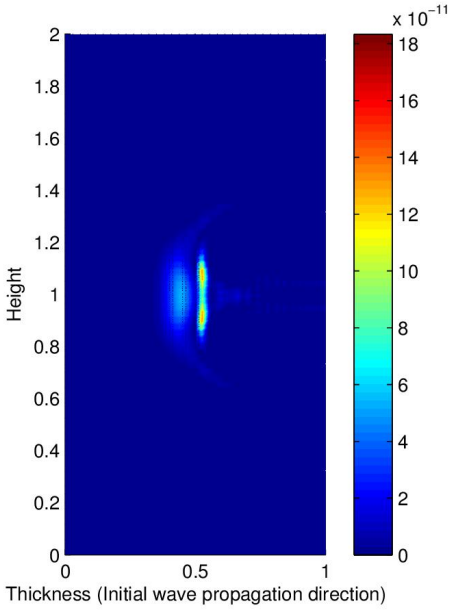

(c) At 1.0 units of time the propagation has reached the interface. Reflection and transmissions occur at the interface region.

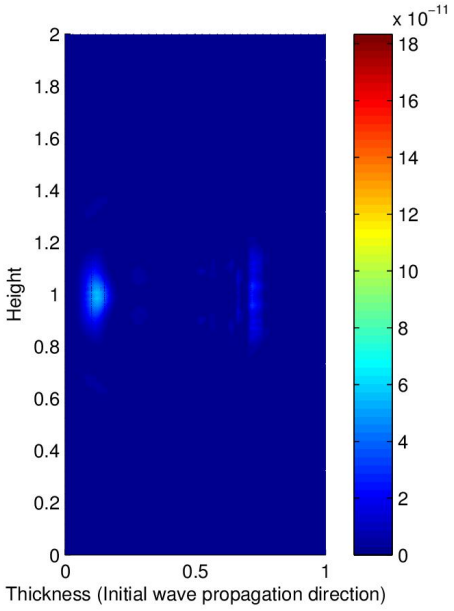

(d) At 1.4 units of time the transmitted wave has reached the wall.

Figure 4.15: Comparison of the nondimensionalized kinetic energy for PC/PU at different instants of time. The kinetic energy decreases by 54.19% as it gets transmitted to the PC layer from PU layer.

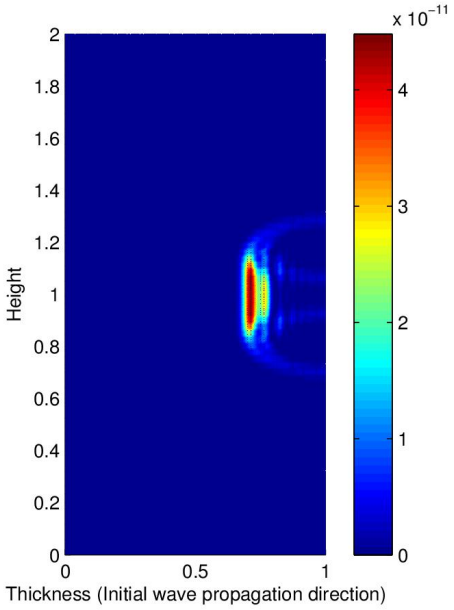

(a) At 0.3 units of time the propagation is same as observed in pure PC layer.

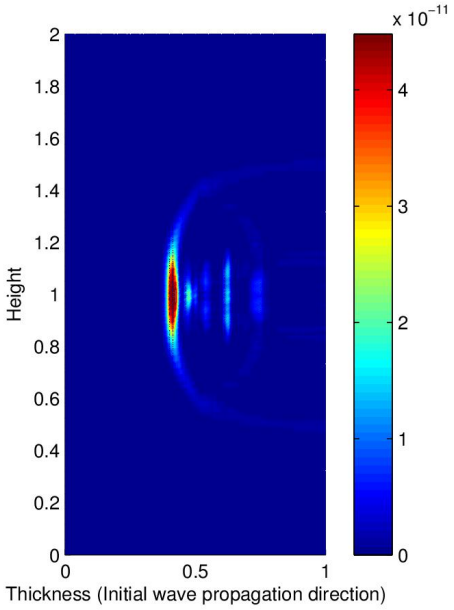

(b) At 0.65 units of time the wave has reached the interface and reflection and transmission of waves occur.

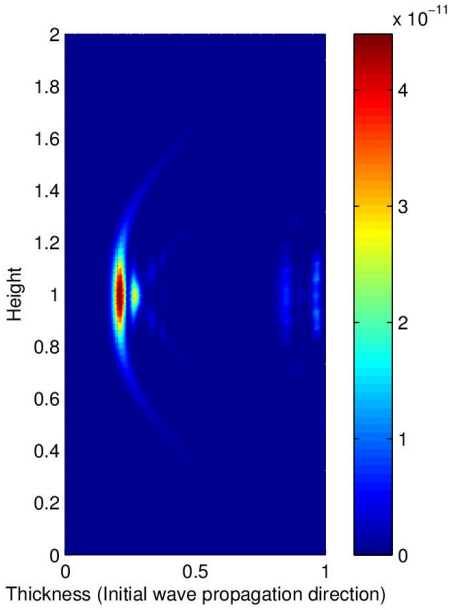

(c) The propagation through the bilayer at 1.0 units of time.

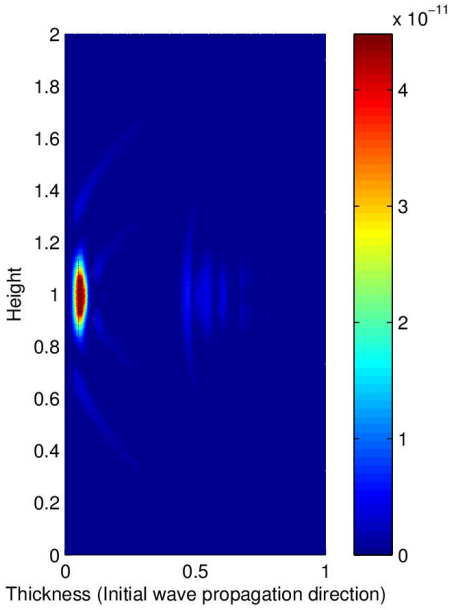

(d) At 1.4 units of time the wave has reached the opposite face of impact.

Figure 4.16: Comparison of the nondimensionalized kinetic energy for PU/PC at two different instants of time. The kinetic energy decreases by 14.06% as it gets transmitted into the PU layer from the PC layer

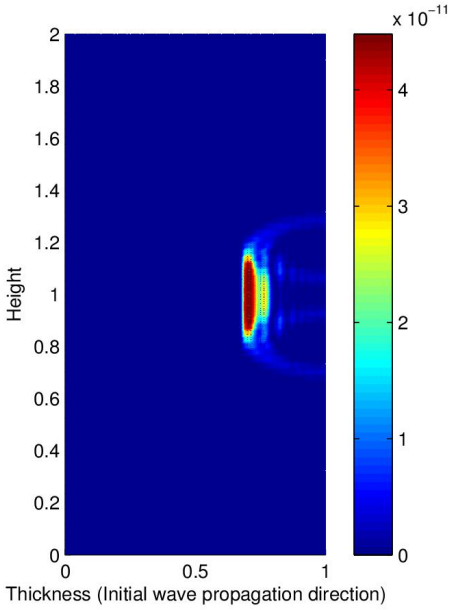

(a) At 0.3 units of time the wave has reached the interface near the impact region. Reflections and transmission of waves occur.

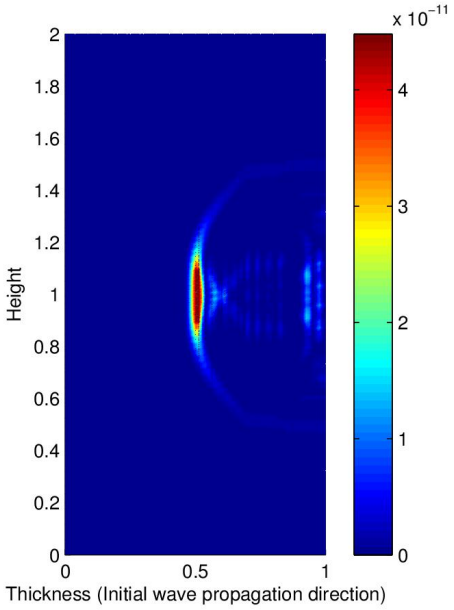

(b) At 0.65 units of time the transmitted wave has reached the center of the domain.

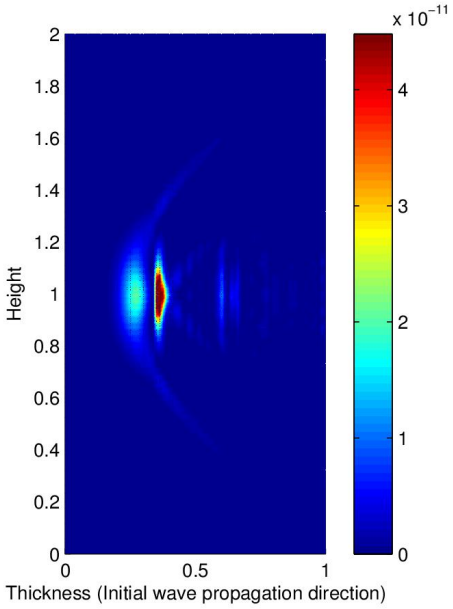

(c) At 1.0 units of time transmitted wave has reached the second interface and multiple reflections and transmissions occur.

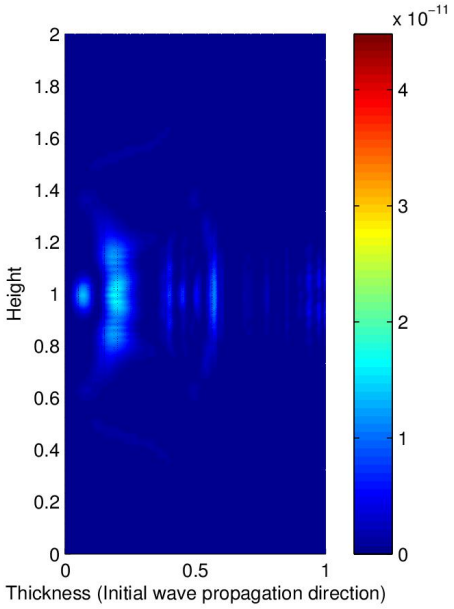

(d) At 1.4 units of time the transmitted wave has reached the opposite face of impact. Multiple reflection and transmission occur due to the interaction at both the interfaces.

Figure 4.17: Comparison of the nondimensionalized kinetic energy for PC/PU/PC at two different instants of time. The reduction of kinetic energy as it gets transmitted into PU from PC layer(near impact side) and into PC from PU layer(near wall) by 29.04% and 75.55%, respectively.

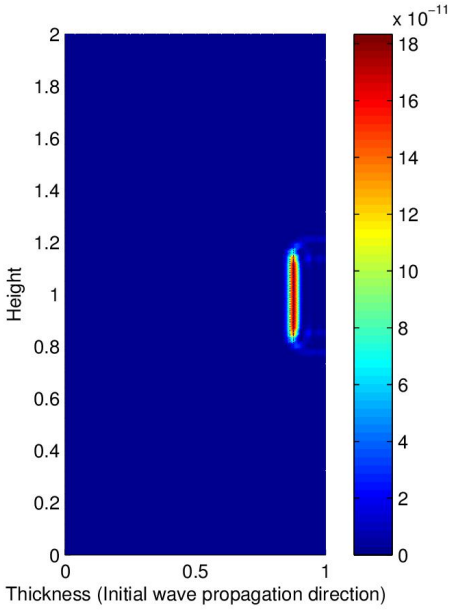

(a) At 0.3 units of time the wave is propagating through the pure PU layer.

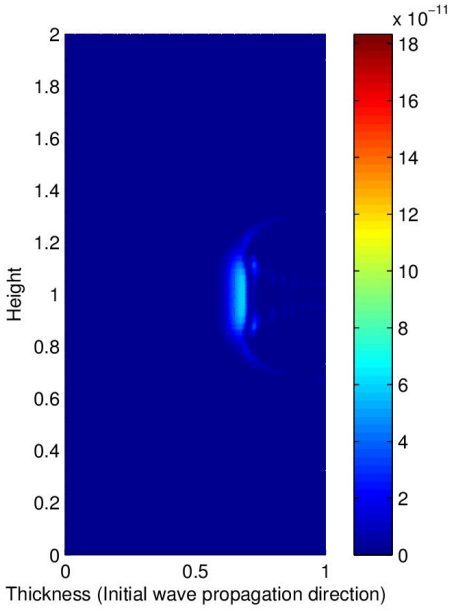

(b) At 0.65 units of time the wave has interacted with the first interface. Reflection and transmission of waves occur.

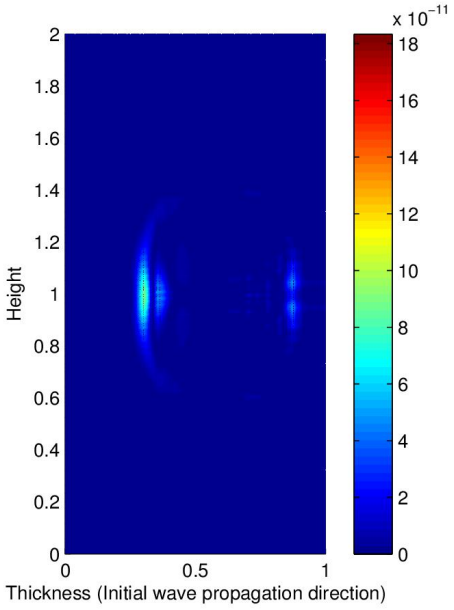

(c) At 1.0 units of time the wave has reached the second interface. Multiple reflection and transmission of wave occur at the interface.

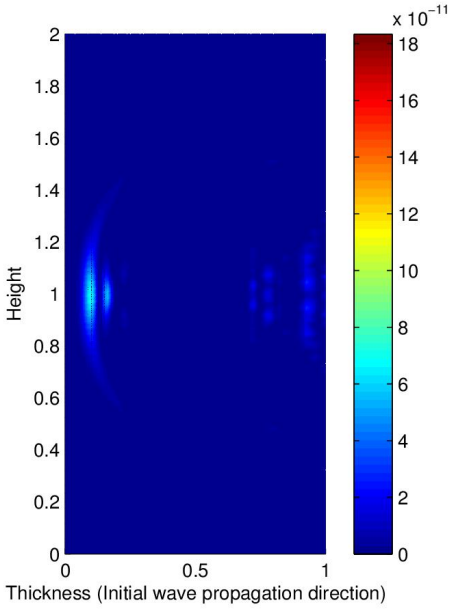

(d) At 1.4 units of time the wave has reached the opposite face of impact. Multiple reflection and transmission of waves occur.

Figure 4.18: Comparison of the nondimensionalized kinetic energy for PU/PC/PU at two different instants of time. The reduction of kinetic energy as it gets transmitted to PC from PU layer(near impact side) and into PU from PC layer(near wall) by 62.96% and 12.13%, respectively.

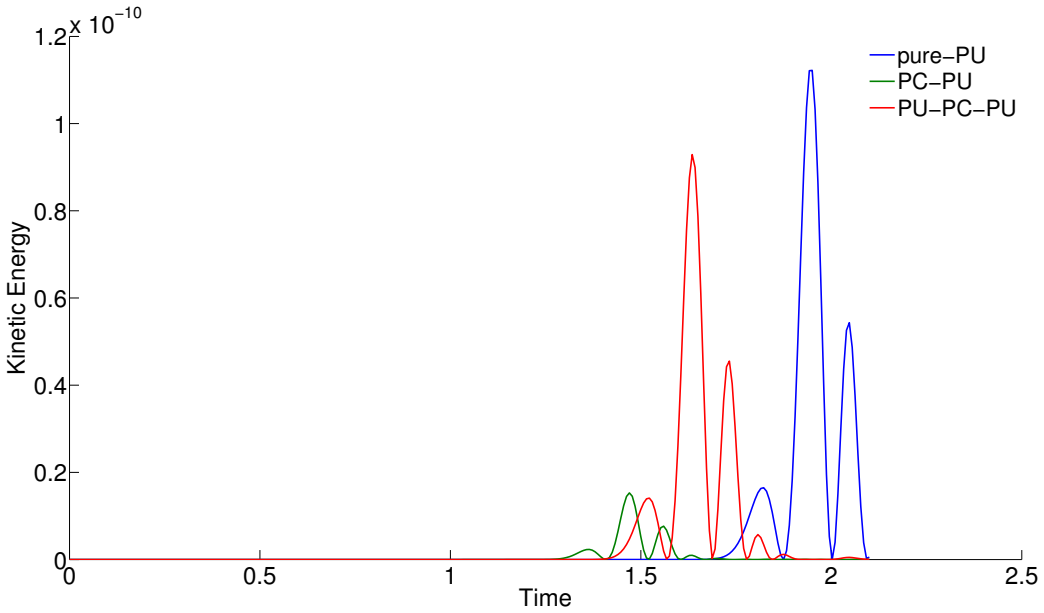

Figure 4.19: Kinetic energy at the wall when PU is impacted

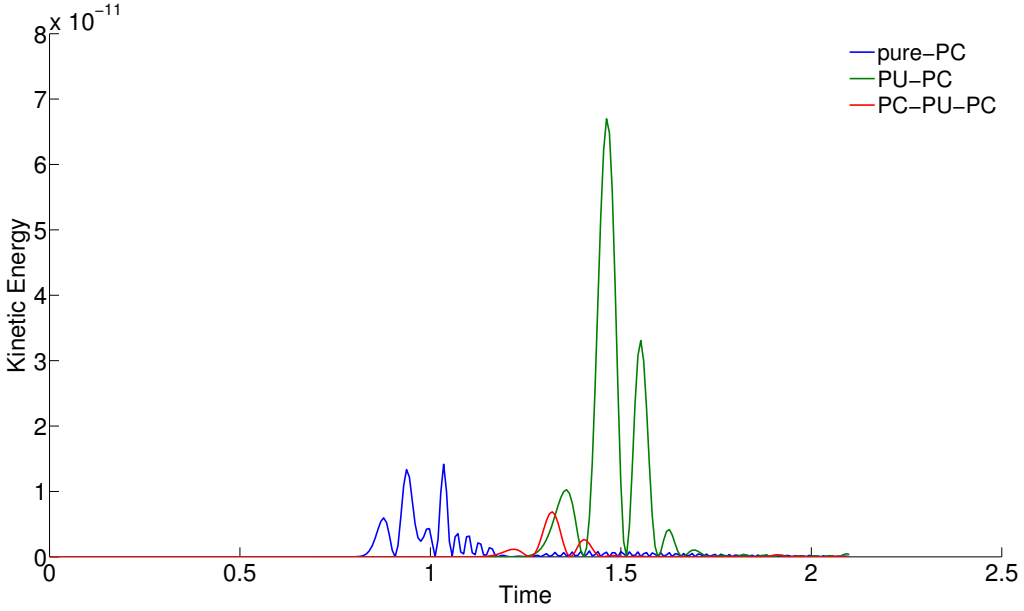

Figure 4.20: Kinetic energy at the wall when PC is impacted

5. FINITE STRAIN MODEL

This chapter deals with the focus on the use of a thermodynamically consistent finite deformation continuum model to simulate the impact response of layered polymer using a three dimensional framework developed by [30]. The thermal phenomena in the above framework is suppressed. The polymer is modeled as a isotropic viscoelastic material. The polymer composite subjected to impact are capable of exhibiting large deformations. Until now we have worked with the assumption of linearized strain and evaluated the small strain response of layered polymer. However, many real world applications involve large strains and therefore it becomes important to develop a finite deformation model for the impact response of layered polymer.

5.1 Constitutive equations

The governing equations used in this study are as follows: The balance of linear momentum is given by

$$\rho_0 \frac{\partial v}{\partial t} = Div\mathbf{P} \tag{5.1}$$

where ρ_0 is the mass density per unit reference volume, $\mathbf{P}$ is the first Piola kirchoff stress and v is the velocity. From the balance of angular momentum, we have

$$\mathbf{S} = \mathbf{F}^{-1}\mathbf{P} = \mathbf{P}^t\mathbf{F}^{-t} \tag{5.2}$$

where $\mathbf{S}$ is the second Piola kirchoff stress and $\mathbf{F}$ is the deformation gradient. The balance of energy is given by

$$\rho_0 \dot{e} = -Div\mathbf{q} + \mathbf{P}\bullet\dot{\mathbf{F}} = -Div\mathbf{q} + \mathbf{S}\bullet\dot{\mathbf{E}} \tag{5.3}$$

where e is the internal energy perunit volume, $\mathbf{E}$ is the Lagrangian strain and $\mathbf{q}$ represents the heat flux.

The response of the viscoelastic material is modeled using a two network theory based on the maximization of entropy production[30]. It consists of a temporary and a permanent network, the instantaneous response is captured by former and the latter captures the long term behavior. A Gibbs potential involving the temporary and permanent network is of the form

$$G = G_1(\mathbf{S}_1, \theta) + G_2(\mathbf{S}_2, \theta)$$

The stress is represented as the sum of the stresses in both network

$$\mathbf{S} = \mathbf{S}_1 + \mathbf{S}_2 \tag{5.4}$$

From the classical thermodynamic relations, the specific entropy(η) and specific internal energy(e) are given by

$$\eta = -\frac{\partial G}{\partial \theta}, \tag{5.5}$$

$$e = G + \theta\eta - \frac{\partial G}{\partial \mathbf{S}_1}\bullet\mathbf{S}_1 - \frac{\partial G}{\partial \mathbf{S}_2}\bullet\mathbf{S}_2 \tag{5.6}$$

Differentiating the above equation w.r.t time 't'

$$\dot{e}|_{\theta \text{ fixed.}} = -\frac{\partial G}{\partial \mathbf{S}_1}\bullet\dot{\mathbf{S}}_1 - \frac{\partial G}{\partial \mathbf{S}_2}\bullet\dot{\mathbf{S}}_2 - \frac{d}{dt}\left\{\frac{\partial G}{\partial \mathbf{S}_1}\right\}\bullet\mathbf{S}_1 - \frac{d}{dt}\left\{\frac{\partial G}{\partial \mathbf{S}_2}\right\}\bullet\mathbf{S}_2 \tag{5.7}$$

Substituting the above equation in (5.3) and assuming the temperature to be constant we get

$$\xi = 0 \tag{5.8}$$

where ξ is the rate of mechanical dissipation is given by

$$\xi = \mathbf{S}_1 \bullet \dot{\mathbf{E}} + \mathbf{S}_2 \bullet \dot{\mathbf{E}} + \rho_0 \frac{d}{dt}\left\{\frac{\partial G}{\partial \mathbf{S}_1}\right\} \bullet \mathbf{S}_1 + \rho_0 \frac{d}{dt}\left\{\frac{\partial G}{\partial \mathbf{S}_2}\right\} \bullet \mathbf{S}_2 \tag{5.9}$$

$$\xi = \mathbf{S}_1 \bullet \left(\dot{\mathbf{E}} + \rho_0 \frac{d}{dt}\left\{\frac{\partial G}{\partial \mathbf{S}_1}\right\}\right) + \mathbf{S}_2 \bullet \left(\dot{\mathbf{E}} + \rho_0 \frac{d}{dt}\left\{\frac{\partial G}{\partial \mathbf{S}_2}\right\}\right) \tag{5.10}$$

The sufficient condition for the equation (5.8) is obtained based on the response of the temporary and permanent network. The temporary network responds elastically and hence it has no dissipation. Therefore from (5.8) and (5.10), we have

$$\dot{\mathbf{E}} = -\rho_0 \frac{d}{dt}\left\{\frac{\partial G}{\partial \mathbf{S}_1}\right\} \tag{5.11}$$

Similarly, the dissipation in permanent network is a function of stress[30]. Therefore from (5.8) and (5.10)

$$\dot{\mathbf{E}} + \rho_0 \frac{d}{dt}\left\{\frac{\partial G}{\partial \mathbf{S}_2}\right\} = \phi \frac{\partial \xi}{\partial \mathbf{S}_2} \tag{5.12}$$

where

$$\phi = \frac{\xi}{\mathbf{S}_2 \bullet \frac{\partial \xi}{\partial \mathbf{S}_2}} \tag{5.13}$$

The equations (5.11) and (5.12) are sufficient for equation (5.8) to be true.

Assuming a quadratic constitutive relation, we have

$$G(\mathbf{S}_1, \mathbf{S}_2, \theta) = -\frac{1}{2}\left(C_{ijkl} S^{(1)}_{kl} S^{(1)}_{ij} + D_{ijkl} S^{(2)}_{kl} S^{(2)}_{ij}\right) \tag{5.14}$$

$$\xi(\mathbf{S}_2) = K_{ijkl} S^{(2)}_{kl} S^{(2)}_{ij} \tag{5.15}$$

where C_{ijkl} and D_{ijkl} are the fourth order compliance tensor for the two elastic networks, and K_{ijkl} is the viscosity tensor of the transient network.

$$\begin{aligned}\frac{\partial G}{\partial \mathbf{S}_1}|_{\theta \text{ fixed }.} &= \frac{-1}{2}\left(\frac{\partial C_{ijkl}}{\partial S^{(1)}_{mn}} S^{(1)}_{kl} S^{(1)}_{ij} + C_{ijkl}\frac{\partial S^{(1)}_{kl}}{\partial S^{(1)}_{mn}} S^{(1)}_{ij} + C_{ijkl} S^{(1)}_{kl}\frac{\partial S^{(1)}_{ij}}{\partial S^{(1)}_{mn}}\right) \\ &= \frac{-1}{2}\left(C_{ijkl}\delta_{km}\delta_{ln} + C_{ijkl}S^{(1)}_{kl}\delta_{im}\delta_{jn}\right) \\ &= -C_{mnkl}S^{(1)}_{kl} \end{aligned} \tag{5.16}$$

Similarly,

$$\frac{\partial G}{\partial \mathbf{S}_2}|_{\theta \text{ fixed }.} = -D_{mnkl}S^{(2)}_{kl} \tag{5.17}$$

$$\frac{\partial \xi}{\partial \mathbf{S}_2}|_{\theta \text{ fixed }.} = 2K_{klmn}S^{(2)}_{kl}S^{(2)}_{ab}S^{(2)}_{ab} + 2K_{ijkl}S^{(2)}_{kl}S^{(2)}_{ij}S^{(2)}_{mn} \tag{5.18}$$

Therefore from equations (5.11) and (5.16), we have

$$\dot{E}_{mn} = \rho_0 C_{mnkl}\dot{S}^{(1)}_{kl} \tag{5.19}$$

and from equations (5.17), (5.18) and (5.12), we have

$$\dot{E}_{mn} = \rho_0 D_{mnkl}\dot{S}^{(2)}_{kl} + \frac{1}{2}\left(K_{klmn}S^{(2)}_{kl}S^{(2)}_{ab}S^{(2)}_{ab} + K_{ijkl}S^{(2)}_{kl}S^{(2)}_{ij}S^{(2)}_{mn}\right) \tag{5.20}$$

where

$$\dot{E}_{mn} = \frac{\partial v_k}{\partial X_m}\frac{\partial u_k}{\partial X_n} + \frac{\partial u_k}{\partial X_m}\frac{\partial v_k}{\partial X_n} + \frac{\partial v_n}{\partial X_m} + \frac{\partial v_m}{\partial X_n} \tag{5.21}$$

where 'u' and 'v' represents displacement and velocity. From conservation of linear

momentum

$$\rho_0 \frac{\partial \mathbf{v}}{\partial t} = Div\mathbf{P} \tag{5.22}$$

$$\mathbf{S} = \mathbf{F}^{-1}\mathbf{P} \tag{5.23}$$

$$\Rightarrow \mathbf{P} = \mathbf{FS} \tag{5.24}$$

$$P_{ij} = F_{ik}S_{kj} \tag{5.25}$$

$$= \frac{\partial u_i}{\partial X_k} S_{kj} + S_{ij} \tag{5.26}$$

$$\therefore \rho_0 \frac{\partial v_i}{\partial t} = \frac{\partial}{\partial X_p}\left(\frac{\partial u_i}{\partial X_k} S_{kp} + S_{ip}\right) \tag{5.27}$$

The final equations used in this study are

$$\therefore \rho_0 \frac{\partial \mathbf{v}}{\partial t} = Div\left((\nabla \mathbf{u})\mathbf{S} + \mathbf{S}\right)$$

$$\mathbf{S} = \mathbf{S}^{(1)} + \mathbf{S}^{(2)} \tag{5.28}$$

$$\dot{\mathbf{S}}^{(1)} = \frac{\tilde{\mathbb{C}}}{\rho_0}\dot{\mathbf{E}} \tag{5.29}$$

$$\dot{\mathbf{S}}^{(2)} = \frac{\tilde{\mathbb{D}}}{\rho_0}\dot{\mathbf{E}} - \frac{1}{2\rho_0}\left(\left(\mathbf{S}^{(2)}\bullet\mathbf{S}^{(2)}\right)\tilde{\mathbb{K}}[\mathbf{S}^{(2)}] + \left(\tilde{\mathbb{K}}[\mathbf{S}^{(2)}]\bullet\mathbf{S}^{(2)}\right)\mathbf{S}^{(2)}\right) \tag{5.30}$$

5.2 Nondimensionalization

To study the influence of the material parameters in the model we nondimensionalize the equations (5.28),(5.29) and (5.30). The characteristic scales used in this study are as follows: $\mathbf{u}$=$L_0\bar{\mathbf{u}}$;$\mathbf{v}$=$v_0\bar{\mathbf{v}}$; t=$t_0\bar{t}$ and $\mathbf{S}$=$J\bar{\mathbf{S}}$ where $\mathcal{J} = \frac{\tilde{\mathcal{C}}_{1111}+\tilde{\mathcal{D}}_{1111}}{\rho_0}$

From equation (5.28), we have

$$\frac{\rho_0 v_0}{t_0}\frac{\partial \bar{v}_i}{\partial \bar{t}} = \frac{J}{L_0}\frac{\partial}{\partial \bar{X}_p}\left(\frac{\partial \bar{u}_i}{\partial \bar{X}_k}\bar{S}_{kp} + \bar{S}_{ip}\right) \tag{5.31}$$

Let us assume $\frac{Jt_0^2}{L_0^2\rho_0} = 1$. $\therefore t_0 = L_0\sqrt{(\rho_0/\mathcal{J})}$ where t_0 is the time taken for the wave to travel a length, 'L_0' through a material of modulus, 'J' and density, 'ρ_0'. Then,

$$\frac{\partial \bar{v}_i}{\partial \bar{t}} = \frac{\partial}{\partial \bar{X}_p}\left(\frac{\partial \bar{u}_i}{\partial \bar{X}_k}\bar{S}_{kp} + \bar{S}_{ip}\right) \tag{5.32}$$

The nondimensionalization of the constitutive equation is given by

$$\dot{\bar{S}}^{(1)}_{ab} = \mathfrak{C}_{abmn}\dot{\bar{E}}_{mn} \tag{5.33}$$

$$\dot{\bar{S}}^{(2)}_{ab} = \mathfrak{D}_{mnkl}\dot{\bar{E}}_{mn} - \left(\mathfrak{K}_{klab}\bar{S}^{(2)}_{kl}\bar{S}^{(2)}_{mn}\bar{S}^{(2)}_{mn} + \mathfrak{K}_{ijkl}\bar{S}^{(2)}_{kl}\bar{S}^{(2)}_{ij}\bar{S}^{(2)}_{ab}\right) \tag{5.34}$$

where $\mathfrak{C}_{abmn} = \frac{\tilde{\mathcal{C}}_{abmn}}{J\rho_0}$,$\mathfrak{D}_{mnkl} = \frac{\tilde{\mathcal{D}}_{mnkl}}{J\rho_0}$ and $\mathfrak{K}_{klab} = \frac{\tilde{\mathcal{K}}_{klab}J^3}{2J\rho_0}$

5.3 Solution technique

The finite volume method was used to solve the above nondimensionalized equations. Let v_1, v_2 and v_3 denote the x, y and z component of velocity. Integrating the momentum equation (5.32) in the x-direction over the 'v_1' velocity control volume dV_P (see figure 5.1), we obtain

$$\int_{CV}\frac{\partial \bar{v}_1}{\partial \bar{t}}dV_P = \int_{CV}\frac{\partial}{\partial \bar{X}_p}\left(\frac{\partial \bar{u}_1}{\partial \bar{X}_k}\bar{S}_{kp} + \bar{S}_{1p}\right)dV_P \tag{5.35}$$

Similarly, the momentum equation in y-direction and z-direction are integrated over the v_2 and v_3 velocity control volume respectively. The displacement and velocity gradients in the constitutive equation (5.33) and (5.34) are approximated using

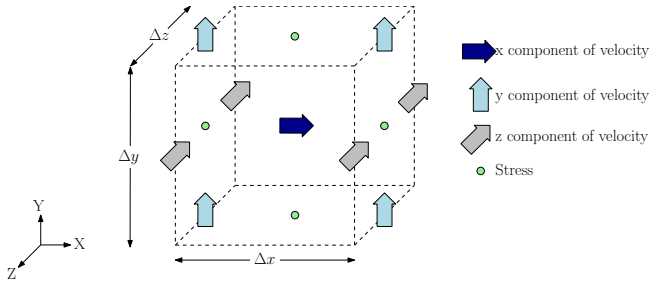

Figure 5.1: Sample 'v_1' control volume.

central difference formula with equal weightage for the nodes on the either side. The discretized equations are solved using FORTRAN®.

5.4 Material parameters

The material parameters used in this study are based on the one dimensional creep and relaxation response of PC [1] and PU [32] respectively which were obtained from literature. Since we use a finite strain model, the material parameter used here is also based on the experiments which involves large strain values. The creep experiment was conducted at 80°C for 1000 seconds at a constant stress of 25 Mpa. The relaxation experiment was conducted at room temperature for a 560 seconds at constant strain of 100%. Figures 5.2 and 5.3 show comparison of the experimental results obtained from literature and that of the implicit model used in this study. The constitutive equations (5.33) and (5.34) are three dimensional but the material parameter obtained from literature is based on the one dimensional response. We assume the material is isotropic and hence two parameters are required to represent the fourth order compliance tensors in the constitutive equations. So we use the Poisson's ratio of 0.45 for PU [40] and 0.37 for PC [31] to find the second parameter. Let λ_i, μ_i(where i=1,2,3) be the two parameters to represent the isotropic tensors $\mathfrak{C}_{abmn}$, $\mathfrak{D}_{abmn}$ and $\mathfrak{K}_{abmn}$ respectively. The tables 5.1 and 5.2 shows the material

parameter used in this finite deformation analysis.

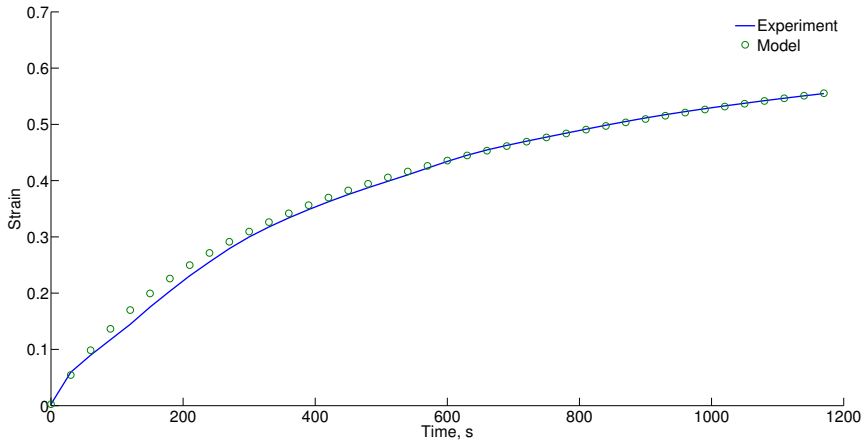

Figure 5.2: Experiments on PC[1] compared with the prediction of the implicit model presented here.

Table 5.1: Material parameters for PU

	λ_i^{PU}	μ_i^{PU}
i=1	2.77189	0.93835
i=2	4.24880	1.43831
i=3	0.00722	0.002443

Table 5.2: Material parameters for PC

	λ_i^{PC}	μ_i^{PC}
i=1	1.797534	0.65603
i=2	0.490360	0.17896
i=3	1.7601e-6	6.423e-7

5.5 Problem description

In this study, we consider a plate of length 'L', height 'H' and thickness 'B'. Along the thickness, different layering sequences as discussed earlier is used. The impact condition is simulated by applying the stress(see figure 4.3) in the localized

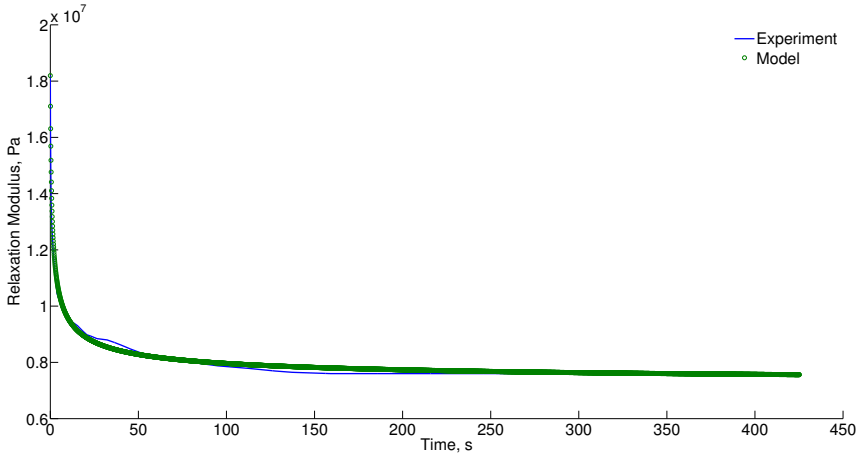

Figure 5.3: Experiments for PU[32] compared with the prediction of the implicit model presented here.

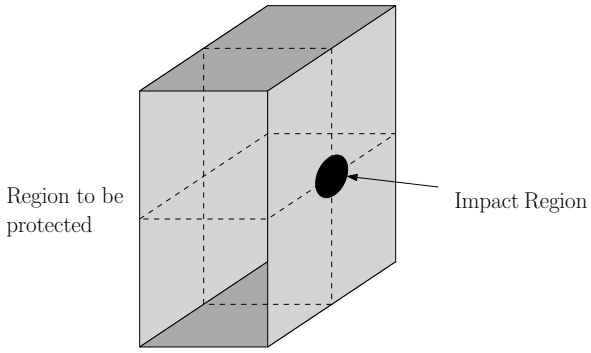

Figure 5.4: Finite Domain of dimensions L x B x H, the impact region is circular region of radius 'r'.

circular region of radius 'r' in one face and the opposite face is fixed(region to be protected see figure 5.4).The initial conditions are

$$\begin{aligned} \mathbf{T}(x,y,z,t) &= \mathbf{0}, \\ v_1(x,y,x,t) &= v_2(x,y,z,t) = v_3(x,y,z,t) = 0 \quad \forall t <= 0. \end{aligned}$$

The boundary condition for the circular impact region is as shown in figure 5.5,

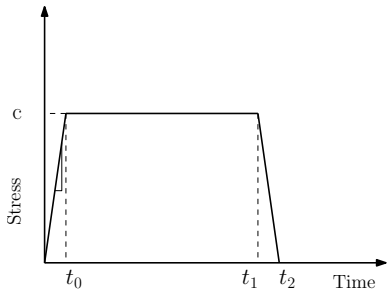

Figure 5.5: Temporal boundary condition for the localized impact region.

the opposite face of impact is fixed and the remaining region is stress free.

5.6 Results and discussions

The propagation of normalized kinetic energy at six different cases considered in this study are shown in figures 5.6 through 5.11 at different instants of time. Reflection and transmission of waves at the interface were captured. The figures 5.6 and 5.7 represent the kinetic energy through pure PC and pure PU layer. From the material data used in the finite model PC is compliant compared to PU, hence the propagation is faster through PU. It can be observed that at 0.5 units of time the influence has not reached the center of the domain whereas in case of PU, it has reflected from the wall and reached the center of the domain. The figures 5.8 and 5.9 shows the propagation through bilayer PU/PC and PC/PU when PC and PU layer are impacted respectively. As the kinetic energy is incident at the interface, partly gets reflected and partly gets transmitted through the interface. In case of bilayer PU/PC, the energy decreases by 51.28% whereas in case of PC/PU energy decreases by 18.40%. Figures 5.10 and 5.11 show the propagation through the trilayer PU/PC/PU and PC/PU/PC at 0.8 units of time when PU and PC are impacted respectively. Since the trilayer involves two interfaces there are multiple reflections and transmission as the energy propagates. In case of trilayer PU/PC/PU the energy

decreases by 19.04% as it gets transmitted at the first interface(near impact region) and by 56.30% as it gets transmitted at the second interface(near wall). In case of trilayer PC/PU/PC the energy decreases by 54.27% as it gets transmitted at the first interface(near impact region) and by 13.51% as it gets transmitted at the second interface(near wall). The main objective on the use of layered composite is to reduce the kinetic energy being transferred on the wall. Figures 5.12 and 5.13 show the kinetic energy on the wall with time when PC and PU is impacted respectively. From the finite strain study conducted the magnitude of kinetic energy on the wall in ascending order is as follows PU/PC/PU, PU/PC, pure PU, PC/PU, PC/PU/PC and pure PC. The order of performance is not the same as observed in the one dimensional and two dimensional model discussed earlier due to interaction through the three dimensional domain. But the best performance in terms of kinetic energy transferred on the wall, is trilayer(PU/PC/PU) which has a compliant layer between two stiff layers, same as observed in the one and two dimensional small strain model.

5.7 Conclusion

The finite deformation impact response of the layered polymer composite was studied using a implicit thermodynamic framework with material parameters obtained from literature and the resulting equations was solved using FVM. A systematic study was conducted for individual layer, bilayer and trilayer polymers of PU and PC. Different layering sequences were considered and it was found that PU/PC/PU sequence provided the best protection as measured by the fraction of input kinetic energy that was transmitted through the shield.

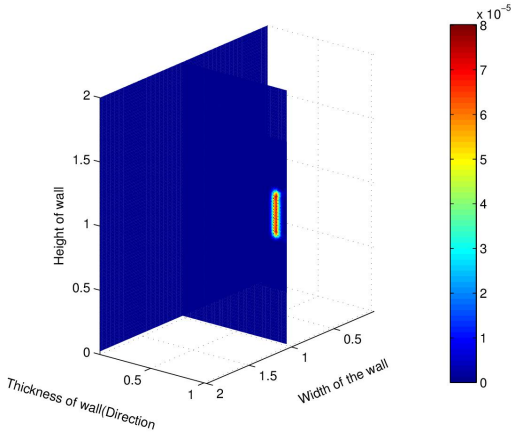

(a) At 0.15 units of time when PC is impacted. The parabolic profile of the wave propagation with high intensity at the center with decreasing intensity away from the center.

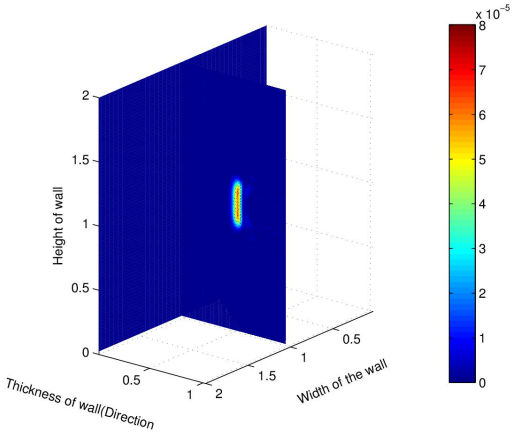

(b) At 0.5 units of time when PC is impacted. Reflection from the wall with the amplitude reduced.

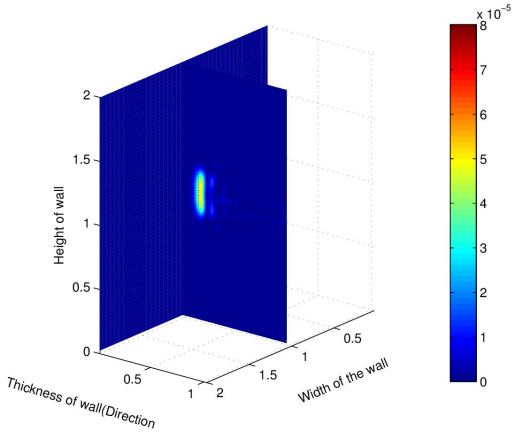

(c) At 0.9 units of time when PC is impacted. The parabolic profile of the wave propagation with high intensity at the center with decreasing intensity away from the center.

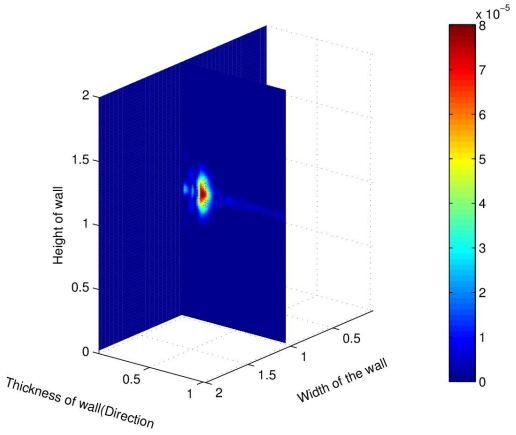

(d) At 1.3 units of time when PC is impacted. Reflection from the wall with the amplitude reduced.

Figure 5.6: The propagation of kinetic energy at 0.5 units of time when PC is impacted. The propagation has crossed the center of the domain. It can be observed that the propagation is slower in PC compared to PU.

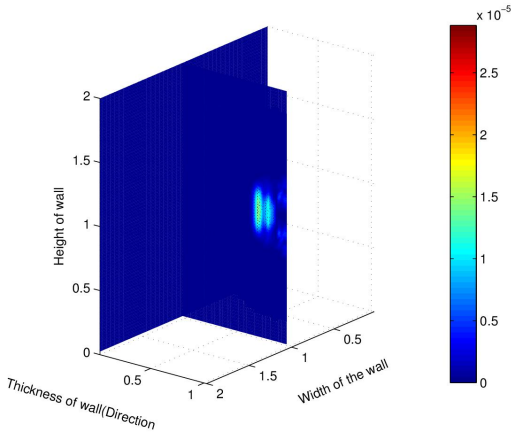

(a) At 0.15 units of time the wave has not reached the center of the domain.

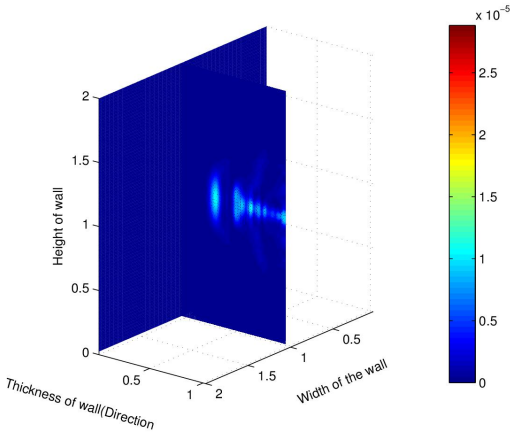

(b) At 0.35 units of time the wave has crossed the center of the domain.

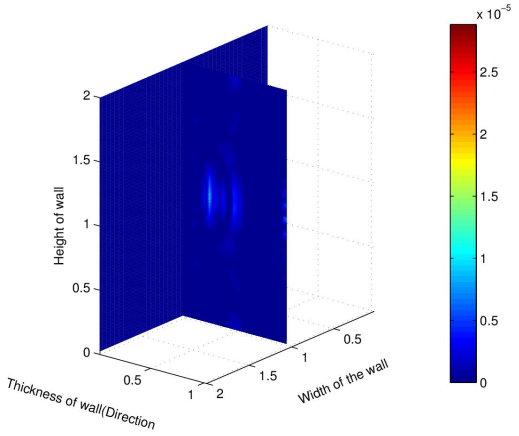

(c) At 0.5 units of time the wave has not reached the center of the domain.

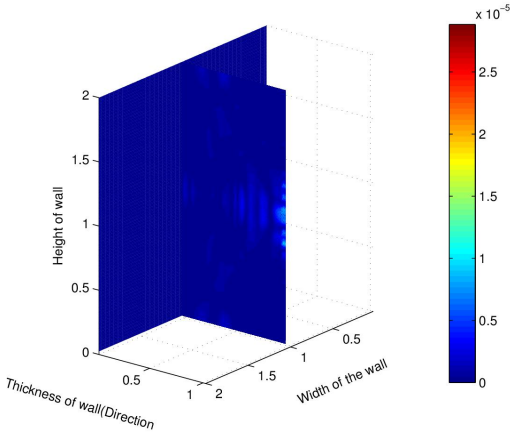

(d) At 0.9 units of time the wave has crossed the center of the domain.

Figure 5.7: The propagation of kinetic energy at 0.5 units of time when PU is impacted. The parabolic profile of the wave propagation with high intensity at the center with decreasing intensity away from the center.

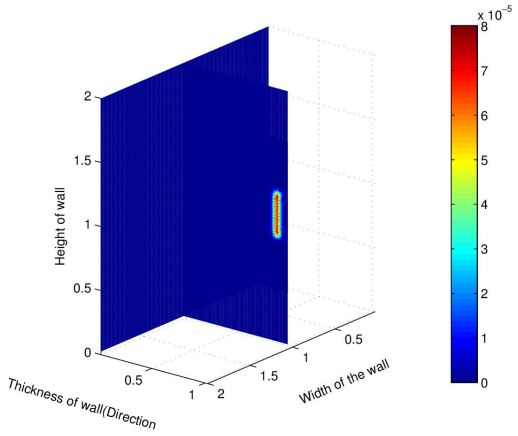

(a) The propagation through the bilayer at 0.15 units of time.

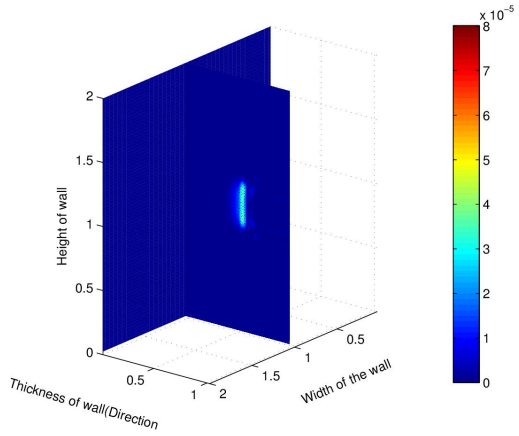

(b) At 0.5 units of time the wave has almost reached the interface of the bilayer PU/PC.

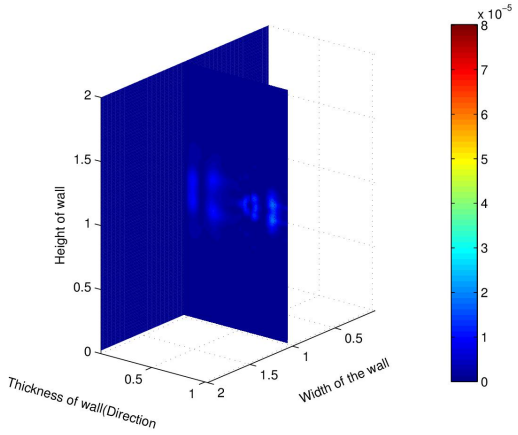

(c) The propagation through the bilayer at 0.9 units of time. Reflection and transmission of the waves occur at the interface.

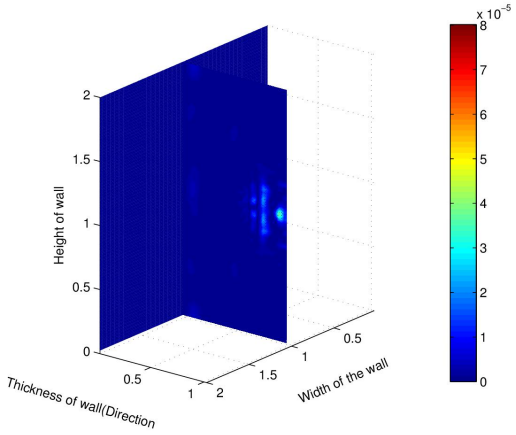

(d) At 1.2 units of time multiple reflection and transmission of wave occurs in the bilayer PU/PC.

Figure 5.8: The propagation of the nondimensionalized kinetic energy through the bilayer PU/PC, at 0.9 units. Since it has not reached the interface there are no reflection. The kinetic energy decreases by 51.28% as it gets transmitted to the PU layer from PC layer.

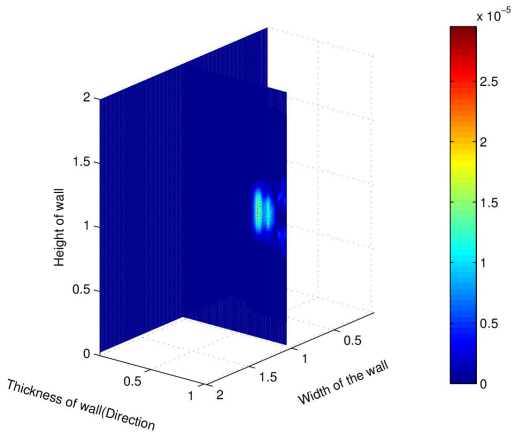

(a) At 0.15 units of time the wave has not reached the center of the domain.

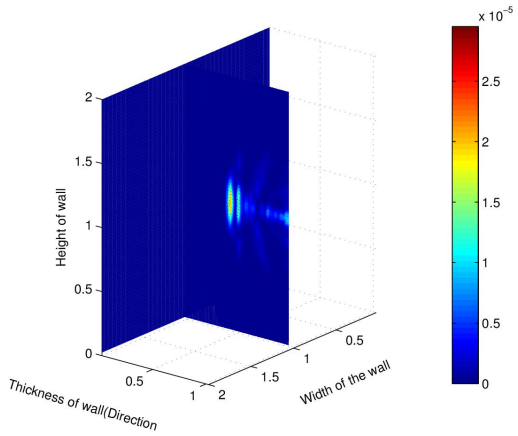

(b) At 0.3 units of time the wave has reached the interface. Reflection and transmission of waves occur.

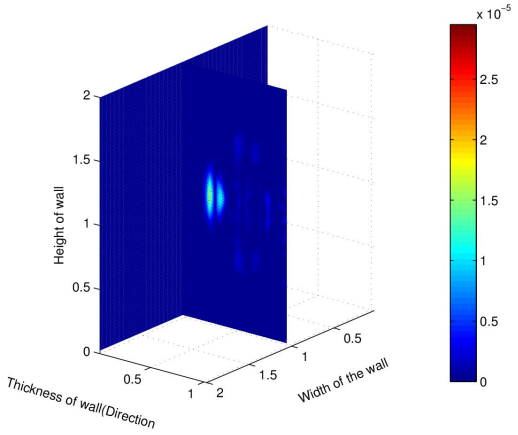

(c) At 0.5 units of time the wave has not reached the almost reached the wall.

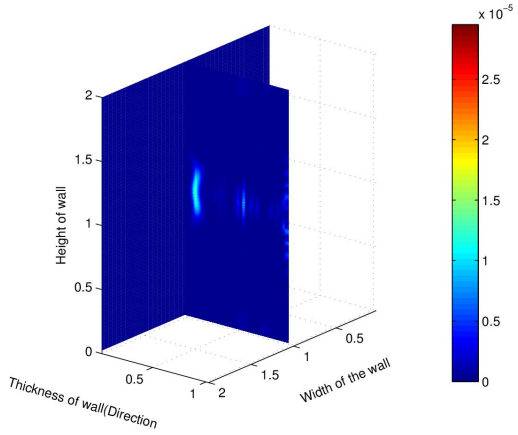

(d) At 0.9 units of time the wave has reflected from the wall.

Figure 5.9: When the nondimensionalized kinetic energy has crossed the interface of the bilayer PC/PU. The kinetic energy decreases by 18.40% as it gets transmitted into the PC layer from the PU layer.

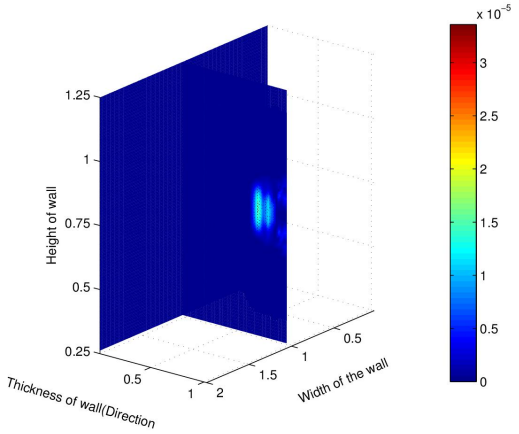

(a) At 0.15 units of time the wave has not reached the first interface since the propagation through PU layer is slow.

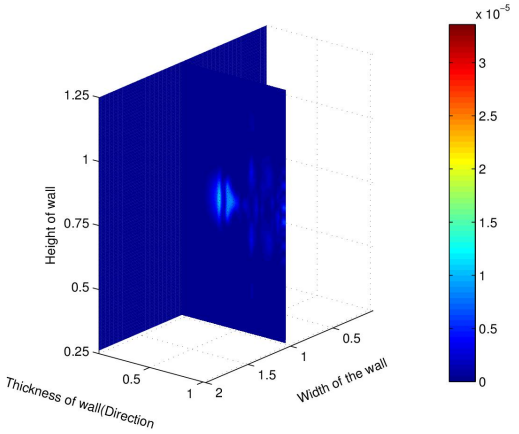

(b) At 0.5 units of time, the wave has interacted with the first interface. Reflection and transmissions of wave occur at the interface.

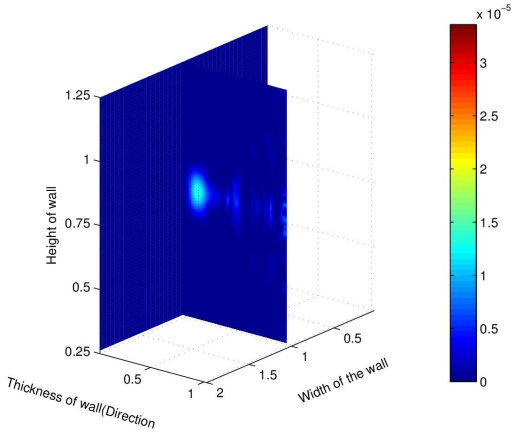

(c) At 0.7 units of time, the transmitted wave has reached the second interface. Multiple reflection and transmission of waves occur.

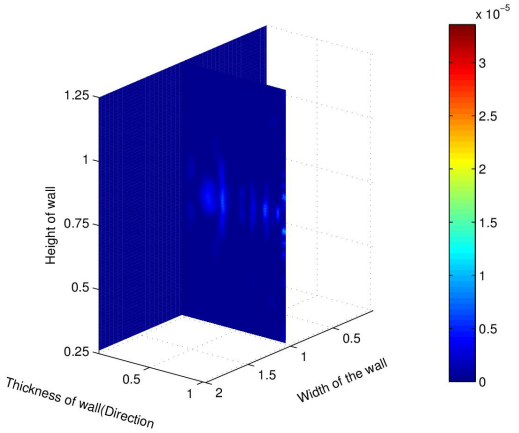

(d) At 0.9 units of time, multiple reflection and transmission of waves occur at the interfaces.

Figure 5.10: At 0.8 units of time, the nondimensionalized kinetic energy has interacted with both the interfaces and multiple reflection and transmissions occur at PU/PC/PU. The kinetic energy reduces by 19.04% as it gets transmitted into PC from PU layer(near impact side) and by 56.30% as it transmitted into PU from PC(near wall).

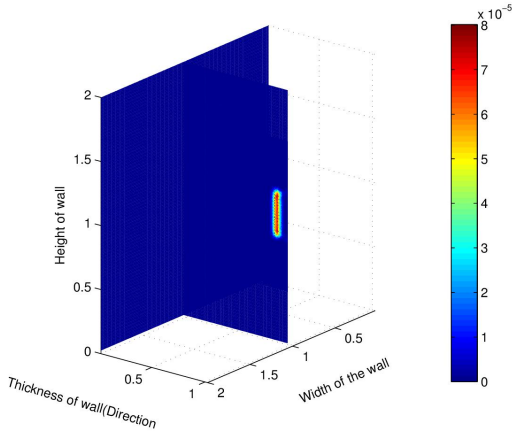

(a) At 0.15 units of time the wave is through PC.

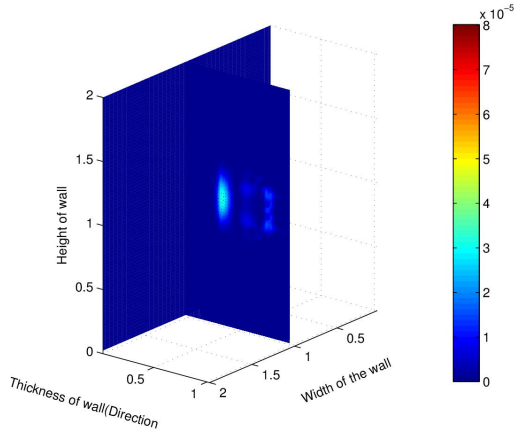

(b) At 0.5 units of time the wave is reached the interface. Reflection and transmission occur due to the interaction at the interfaces.

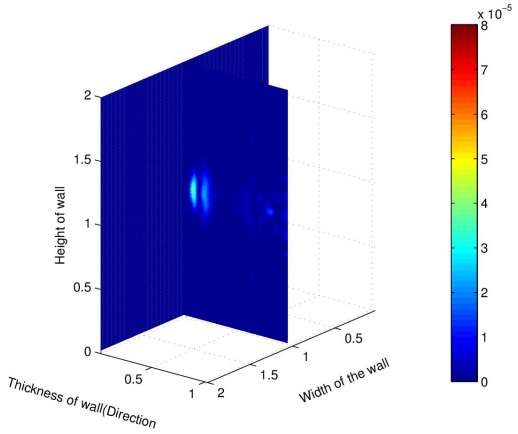

(c) At 1.0 units of time the transmitted wave has reached the second interface. Reflection and transmission of wave reaches the second interface.

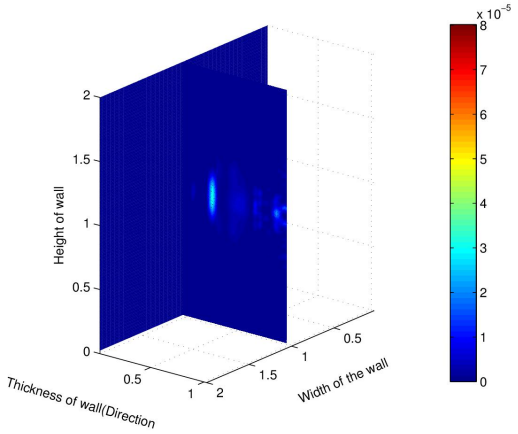

(d) At 1.2 units of time multiple reflection and transmission occur due to the interaction at both the interfaces.

Figure 5.11: At 0.8 units of time,the nondimensionalized kinetic energy has interacted with both the interfaces and multiple reflection and transmissions occur at PC/PU/PC. The kinetic energy reduces by 54.27% as it gets transmitted into PU from PC layer(near impact side) and by 13.51% as it transmitted into PC from PU(near wall).

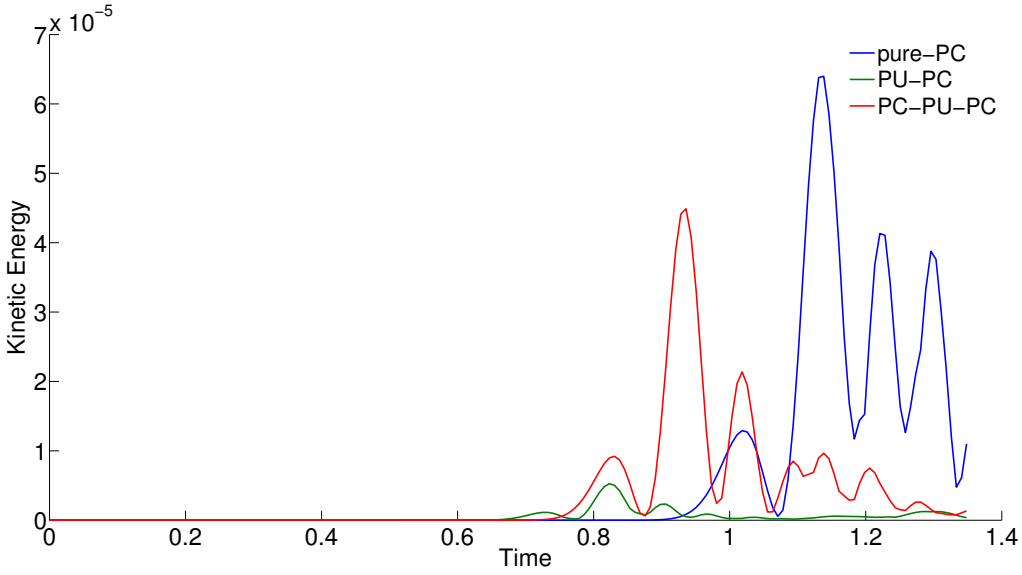

Figure 5.12: Kinetic energy at the wall when PC is impacted

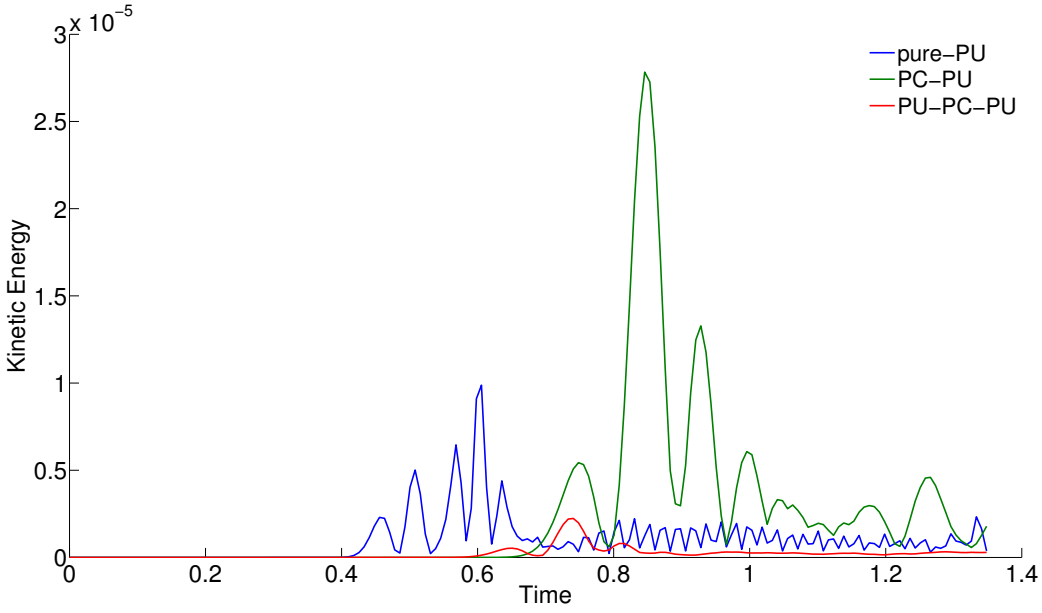

Figure 5.13: Kinetic energy at the wall when PU is impacted

6. CONCLUSION

6.1 Conclusion on the small strain one dimensional and two dimensional model

A thermodynamically consistent framework was used to study impact response of layered polymeric plate involving small deformation with the thermal phenomena suppressed. Even though the strains were small, the response was assumed to be nonlinear. Using a nonlinear dashpot we were able to capture the long term response of polymers better, with less number of parameters, compared to the integral models involving Prony series and rate type models based on spring and dashpot combinations. Impact of a large layered plate with infinite dimensions in two directions and finite dimension in one direction was studied using one dimensional model and plate with inifinite dimension in one direction and finite dimension in two directions was studied using the two dimensional model. Six different protocols such as pure PC, pure PU, bilayer(PU/PC and PC/PU) and trilayer (PU/PC/PU and PC/PU/PC). The interfaces are assumed to be fully bonded. The material parameters were obtained from the experimental found in the literature. Finite volume numerical scheme was used the solve resulting set of governing equations from two network theory. The one dimensional model was able to capture the transmission and reflection phenomenon at the interface. In addition, two dimensional model was able to capture the transmission and interaction of waves across the two dimensional domain. In both one dimensional and two dimensional model, the layering of polymer provided better performance depending upon the layering sequence. The trilayer sequence of PC/PU/PC which was having a compliant layer between two stiff layer had the lowest kinetic energy transferred on the wall. FVM is a viable alternative to study the impact response of layered plate.

6.2 Conclusion on the finite strain model

A thermodynamically consistent finite strain model was used to simulate the impact response of a layered plate with the thermal phenomena being suppressed. The two network theory used here takes into account the essential features of the viscoelastic material, namely instantaneous and the long term response. A specific form for the Gibbs potential was chosen for the two networks such that it is function of stress in each of their network. Similar to the small strain model six protocols were considered. The impact was simulated by applying a stress boundary condition in a circular region in one face of the plate. The reflection and transmission of waves in three dimensional domain occurring at the interfaces were captured using the finite deformation model. The kinetic energy transferred on the wall was lowest when the trilayer of PU/PC/PU. The performance was similar to the small deformation i.e., having a compliant layer between two stiff layers resulted in better performance. One dimensional and two dimensional study is enough to select the layering sequence based on the qualitative analysis. Quantitative comparison of the experimental results cannot be made since the material parameters were not available.

6.3 Recommendations for future work

The following research topic needs attention: The finite strain model used here involves two compliance tensors and a viscosity tensor. A comprehensive experimental studies needs to be carried out to find the parameters of these tensor which can be used to simulate impact response better. The model developed here can also be used to evaluate the performance of anisotropic materials. The thermal phenomena of the three dimensional framework developed by [30] can be included by incorporating suitable adjustments to the Gibbs potential by making it as a function of stress

in both networks and temperature. In addition the compliance tensor and viscosity tensor will also depend on the temperature. Study can also be carried by assuming different friction condition at the interface. The wall can also be modeled to include the dissipation effects. Reflection of the kinetic energy at interface is the important phenomenon in reducing the kinetic energy on wall. This phenomenon can be explored by selecting different periodic interface patterns such as rectangular, circular, triangular, etc(see figure 6.1).

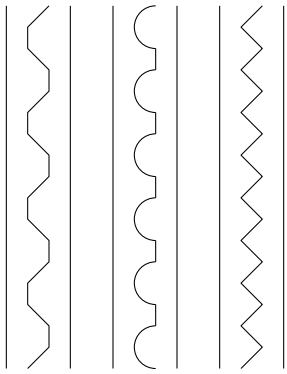

Figure 6.1: Different patterns at the interface

REFERENCES

[1] M. Abu-Abdeen. The unusual effect of temperature on stress relaxation and mechanical creep of polycarbonate at low strain and stress levels. *Materials and Design*, 34:469–473, 2012.

[2] M. R. Amini, J. Simon, and S. Nemat-Nasser. Numerical modeling of effect of polyurea on response of steel plates to impulsive loads in direct pressure-pulse experiments. *Mechanics of Materials*, 42(6):615 – 627, 2010.

[3] M.R. Amini, J.B. Isaacs, and S. Nemat-Nasser. Experimental investigation of response of monolithic and bilayer plates to impulsive loads. *International Journal of Impact Engineering*, 37(1):82–89, January 2010.

[4] A. V. Amirkhizi, J. Isaacs, J. McGee, and S. Nemat-Nasser. An experimentally-based viscoelastic constitutive model for polyurea, including pressure and temperature effects. *Philosophical Magazine*, 86(36):5847–5866, 2006.

[5] J. N. Antonakakis, P. Bhargava, K. C. Chuang, and A. T. Zehnder. Linear viscoelastic properties of HFPE-II-52 polyimide. *Journal of Applied Polymer Science*, 100(4):3255–3263, 2006.

[6] C Bailey and M Cross. A finite volume procedure to solve elastic solid mechanics problems in three dimensions on an unstructured mesh. *International Journal for Numerical Methods in Engineering*, 38:1757–1776, 1995.

[7] I. Bijelonja, I. Demirdžić, and S. Muzaferija. A finite volume method for incompressible linear elasticity. *Computer Methods in Applied Mechanics and Engineering*, 195(44-47):6378–6390, 2006.

[8] J Michael Boteler, A M Rajendran, and David Grove. Shock wave profiles in polymer matrix composite. *AIP Conference Proceedings*, 505(1):563–566, 2000.

[9] T. W. Ching and V. B. C. Tan. Modelling Ballistic Impact on Woven Fabric With LS-DYNA. *Computational Methods*, pages 1879–1884, 2006.

[10] I. Demirdžić, E. Džaferović, and a. Ivanković. Finite-volume approach to thermoviscoelasticity. *Numerical Heat Transfer, Part B: Fundamentals*, 47(3):213–237, 2005.

[11] I Demirdžić, I Horman, and D Martinović. Finite volume analysis of stress and deformation in hygro-thermo-elastic orthotropic body. *Computer Methods in Applied Mechanics and Engineering*, 190:1221–1232, 2000.

[12] P R Eiseman and A P Stone. Conservation laws of fluid dynamics-a survey. *SIAM Review*, 22(1):12–27, 1980.

[13] J. Fainberg and H. J. Leister. Finite volume multigrid solver for thermo-elastic stress analysis in anisotropic materials. *Computer Methods in Applied Mechanics and Engineering*, 137(96):167–174, 1996.

[14] Y.D. Fryer, C. Bailey, M. Cross, and C.-H. Lai. A control volume procedure for solving the elastic stress-strain equations on an unstructured mesh. *Applied Mathematical Modelling*, 15(11-12):639–645, 1991.

[15] S. Gogineni, X. L. Gao, N. V. David, and J. Q. Zheng. Ballistic impact of twaron CT709® plain weave fabrics. *Mechanics of Advanced Materials and Structures*, 19(6):441–452, 2012.

[16] M. Grujicic, B Pandurangan, T He, B A Cheeseman, C Yen, and C L Randow. Computational investigation of impact energy absorption capability of polyurea coatings via deformation-induced glass transition. *Materials Science and Engineering: A*, 527(29-30):7741–7751, 2010.

[17] Rami M. Haj-Ali and Anastasia H. Muliana. Numerical finite element formulation of the schapery non-linear viscoelastic material model. *International Journal for Numerical Methods in Engineering*, 59(1):25–45, 2004.

[18] Jo Hallquist. *LS-DYNA theory manual*. Livermore Software Technology Corporation, 2006.

[19] Zhao Han and Gary Gerard. A three dimensional analytical solution of the longitudinal wave propagation in an infinite linear viscoelastic cylindrical bar. application to experimental techniques. *Journal of the Mechanics and Physics of Solids*, 43(8):1335 – 1348, 1995.

[20] Amit Jain, George Youssef, and Vijay Gupta. Dynamic tensile strength of polyurea-bonded steel/E-glass composite joints. *Journal of Adhesion Science and Technology*, 27(4):403–412, 2013.

[21] Said Jazouli, Wenbo Luo, Fabrice Bremand, and Toan Vu-Khanh. Nonlinear creep behavior of viscoelastic polycarbonate. *Journal of Materials Science*, 41(2):531–536, 2006.

[22] W.G. Knauss and J. Zhao. Improved relaxation time coverage in ramp-strain histories. *Mechanics of Time-Dependent Materials*, 11(3-4):199–216, 2007.

[23] C.T. Lim, V.P.W. Shim, and Y.H. Ng. Finite-element modeling of the ballistic impact of fabric armor. *International Journal of Impact Engineering*, 28(1):13 – 31, 2003.

[24] S. V. Patankar and D. B. Spalding. A calculation procedure for heat, mass and momentum transfer in three-dimensional parabolic flows. *International Journal of Heat and Mass Transfer*, 15:1787–1806, 1972.

[25] Jonathan R. Porter, Mr. Robert J. Dinan, Dr. Michael I. Hammons, and Dr. Kenneth J. Knox. Polymer coatings increase blast resistance of existing and temporary structures. *The AMPTIAC Quarterly*, 6(4):47–52, 2003.

[26] K. R. Rajagopal. On implicit constitutive theories. *Applications of Mathematics*, 48(4):279–319, 2003.

[27] K. R. Rajagopal. The elasticity of elasticity. *Zeitschrift fur Angewandte Math-*

ematik und Physik, 58(2):309–317, 2007.

[28] K. R. Rajagopal. On the nonlinear elastic response of bodies in the small strain range. *Acta Mechanica*, pages 1–9, 2013.

[29] K. R. Rajagopal and A. R. Srinivasa. A Gibbs-potential-based formulation for obtaining the response functions for a class of viscoelastic materials. *Proceedings of the Royal Society A: Mathematical, Physical and Engineering Science*, 467(2125):39–58, 2011.

[30] K. R. Rajagopal and A. R. Srinivasa. An implicit thermomechanical theory based on a Gibbs potential formulation for describing the response of thermoviscoelastic solids. *International Journal of Engineering Science*, 70:15–28, 2013.

[31] Qasim H. Shah. Impact resistance of a rectangular polycarbonate armor plate subjected to single and multiple impacts. *International Journal of Impact Engineering*, 36(9):1128–1135, 2009.

[32] Jongmin Shim and Dirk Mohr. Rate dependent finite strain constitutive model of polyurea. *International Journal of Plasticity*, 27(6):868–886, June 2011.

[33] V.P.W. Shim, V.B.C. Tan, and T.E. Tay. Modelling deformation and damage characteristics of woven fabric under small projectile impact. *International Journal of Impact Engineering*, 16(4):585 – 605, 1995.

[34] A. K. Slone, C. Bailey, and M. Cross. Dynamic solid mechanics using finite volume methods. *Applied Mathematical Modelling*, 27(2):69–87, 2003.

[35] Srinivasan Arjun Tekalur, Arun Shukla, and Kunigal Shivakumar. Blast resistance of polyurea based layered composite materials. *Composite Structures*, 84(3):271 – 281, 2008.

[36] Ž . Tuković, A. Ivanković, and A. Karać. Finite-volume stress analysis in multimaterial linear elastic body. *International Journal for Numerical Methods in*

Engineering, 93(4):400–419, 2013.

[37] M. A. Wheel. A finite-volume approach to the stress analysis of pressurized axisymmetric structures. *International Journal of Pressure Vessels and Piping*, 68(3):311–317, 1996.

[38] A. S. Wineman and K. R. Rajagopal. *Mechanical response of polymers: an introduction*. Cambridge University Press, 2000.

[39] Zhen Yao, Defeng Wu, Chong Chen, and Ming Zhang. Creep behavior of polyurethane nanocomposites with carbon nanotubes. *Composites Part A: Applied Science and Manufacturing*, 50:65–72, 2013.

[40] G. Youssef and V. Gupta. Resonance in polyurea-based multilayer structures subjected to laser-generated stress waves. *Experimental Mechanics*, 53(2):145–154, 2013.